

CO2 Evaporation Process Modelling: Fundamentals and Engineering Applications

CHENG, Lixin, XIA, Guodong and LI, Qinling <<http://orcid.org/0000-0002-7191-9538>>

Available from Sheffield Hallam University Research Archive (SHURA) at:

<https://shura.shu.ac.uk/28398/>

This document is the Accepted Version [AM]

Citation:

CHENG, Lixin, XIA, Guodong and LI, Qinling (2021). CO2 Evaporation Process Modelling: Fundamentals and Engineering Applications. Heat Transfer Engineering, 43 (8-10). [Article]

Copyright and re-use policy

See <http://shura.shu.ac.uk/information.html>

CO₂ Evaporation Process Modelling: Fundamentals and Engineering Applications

Lixin Cheng^{a,b*}, Guodong Xia^a and Qinling Li^b

*^aBeijing Key Laboratory of Heat Transfer and Energy Conversion, Beijing University of Technology,
Beijing 100124, P. R. China*

*^bDepartment of Engineering and Mathematics, Sheffield Hallam University, City Campus, Howard Street,
Sheffield S1 1WB, UK*

This paper presents critical analysis of process modeling and mechanisms of CO₂ evaporation inside macro- and micro-channels. First, some existing experimental results of CO₂ evaporation heat transfer in macro-channels and micro-channels are compared and discussed. Then, the comprehensive two-phase flow pattern map of Cheng et al. for CO₂ evaporation inside channels is presented. The flow pattern map has widely been used to predict flow patterns of CO₂ evaporation processes and favorably agrees with observed CO₂ two phase flow patterns in various channels. Next, the Cheng et al. generalized CO₂ evaporation heat transfer model based on flow patterns is compared to the experimental data. It has been proved that the heat transfer model favorably agrees with the experimental data by many researchers over the past decade. Simulation results of evaporation heat transfer in both macro- and micro-channels using the model are also presented. Furthermore, evaporation heat transfer mechanisms are analyzed from the flow regime variations and unstable evaporation heat transfer characteristics in both macro- and micro-channels. Finally, applications of the Cheng et al. CO₂ evaporation heat transfer model in evaporator design for various thermal

systems are reviewed. Future research needs are identified according to this comprehensive analysis and review,

* Address correspondence to Dr. Lixin Cheng, Department of Engineering and Mathematics, Sheffield Hallam University, City Campus, Howard Street, Sheffield S1 1WB, UK. E-mail: lixincheng@hotmail.com.

Introduction

Over the past decade, CO₂ has been receiving renewed interest as an efficient and environmentally safe working fluid in a number of applications including automotive air conditioning, residential heat pumps, as a primary and secondary refrigerant in refrigeration systems at low temperatures, various energy and power generation systems [1 – 6]. It also has potential applications in cooling for electronic device, particle physics detectors and other high heat flux removal. As the effects of good thermophysical properties, favorably evaporation heat transfer, two-phase flow, supercritical heat transfer and fluid flow characteristics of CO₂, smaller pipe dimensions can be used in its thermal energy systems. Both macro- and micro-channels are used in various CO₂ thermal systems [1, 4, 7]. Furthermore, as a natural working fluid, CO₂ has no ozone depletion potential and a negligible direct global warming potential. Therefore, CO₂ is an ideal working fluid for many thermal and energy engineering applications.

CO₂ has positive attributes as a secondary refrigerant at low temperatures in commercial refrigeration used in supermarkets, shops and large kitchens, in indirect and low temperature cascade systems and as a primary refrigerant in all CO₂ centralized refrigeration systems. Figure 1 shows a schematic of an ammonia-CO₂ secondary loop of an indirect refrigeration system which operates at low temperatures. In this refrigeration system, CO₂ evaporation and condensation processes are nearly at the same pressures. In particular, this system does not involve any oil effect for the CO₂ secondary loop. The main benefits for using CO₂ in indirect system arrangements include the simplicity of the system and the possibility of using components for other refrigerants to build the CO₂ circuit. Furthermore, other arrangements, such as cascade and multistage systems have been used commercially [7]. Advantages of CO₂ cascade systems include greatly reduced low-temperature compressor size, the absence of a liquid pump and fewer stages of heat transfer. For example, two-

stage and multistage CO₂ centralized refrigerant systems are also used in supermarket refrigeration. These systems are most suitable for cold climates or where heat sinks are available [8]. The operation of such refrigeration systems is mostly in the sub-critical region. If the ambient temperature is higher than the critical temperature, the system will be super-critical and this generally should be connected to another thermal system such as hot water or space heating heat pumps for efficient energy use. Due to its excellent safety characteristics (nonflammable, non-explosive, inexpensive and relatively nontoxic), CO₂ is an ideal refrigerant to be used in the refrigerated spaces. Due to the high working pressure, CO₂ as a phase change secondary refrigerant has a high volumetric refrigeration capacity, which equates to approximately five times or more that of R22 and NH₃. Use of CO₂ in these refrigeration systems requires understanding and prediction of convective evaporation and condensation heat transfer, two-phase flow patterns and pressure drops in macro-channels at low temperatures for achieving more accurate designs of evaporators and more energy-efficient cycles using CO₂.

CO₂ has favorable thermal performance when used in air-conditioning and heat pump systems as compared to conventional refrigerants. For example, in the CO₂ automobile air-conditioning system as shown in Fig. 2. For ambient air temperatures, the heat transfer process on the high pressure side of a CO₂ cycle is not a condensation process as in conventional systems but a supercritical gas cooling process [3, 6]. For the evaporation processes in the evaporator, CO₂ evaporates at much higher pressure than conventional refrigerant R134a as shown in the thermal cycles in Fig. 3. The physical and transport properties of CO₂ are quite different from those of conventional refrigerants at the same saturation temperatures. The physical properties have a significant effect on the evaporation processes including the two-phase flow patterns, evaporation heat transfer characteristics and two-phase pressure drops in the compact heat exchangers with micro-channels [1, 3]. Therefore, it is essential to understand the two-phase flow and evaporation processes for properly designing the

evaporators which use micro-scale channels for the automobile air-conditioning and heat pump systems.

Use of CO₂ in various energy systems requires the understanding the characteristics and mechanisms of convective evaporation heat transfer, two-phase flow regimes, pressure drops, supercritical CO₂ heat transfer and fluid flow behaviors in both macro- and micro-channels [6, 8 - 10]. It is also essential to develop proper prediction models for these heat transfer and fluid flow behaviors in order to design evaporators, gas coolers, various components and more energy-efficient thermal cycles using CO₂. Nearly all available prediction methods for evaporation heat transfer are for macro-channels under low reduced pressures and do not apply for CO₂ evaporation processes [9, 11]. The proper prediction models for CO₂ evaporation heat transfer should be relevant to the physical mechanisms and corresponding flow regimes [12 – 16]. To this end, Cheng et al. [17 – 20] developed a comprehensive flow map CO₂ and a generalized mechanistic evaporation heat transfer model based on the flow regimes a decade ago. Since then, many experimental studies on CO₂ evaporation heat transfer and two phase flow have been done. From a predictive standpoint, many features of the existing flow pattern maps and evaporation heat transfer correlations require refinement to attain the desired level of accuracy for CO₂ evaporator design and thermal systems. Therefore, it is the time to analyze the Cheng et al. [17 – 20] evaporation heat transfer model and flow pattern map through comparing to numerous available test data in the literature. It is also essential to review the applications of the model and flow map in various engineering research and practical design including evaporators and thermal systems.

The objectives of this paper are to review and analyze the characteristics of CO₂ evaporation heat transfer, two phase flow patterns and the evaporation model and flow pattern map developed by Cheng et al. [17 – 20]. First, the review addresses the extensive experimental studies on CO₂ evaporation heat transfer and two-phase flow in macro-channels and micro-channels. Then, studies

of CO₂ two-phase flow patterns are summarized and the flow pattern map specially for CO₂, which cover both macro- and micro- channels developed by Cheng et al. [17, 19] is discussed. The generalized mechanistic heat transfer model for CO₂ evaporation heat transfer of CO₂ is presented and compared to the experimental data in the literature. Some simulation results are presented. In the engineering application aspect, comparison of simulation results and the experimental data in the real thermal systems are presented. Furthermore, potential application of CO₂ for high heat flux cooling, thermal and power systems are also discussed. The future research needs are identified according to this comprehensive analysis and review.

Distinction criteria between macro- and micro-Channels

Both macro- and micro-scale channels are used in the CO₂ refrigeration, air-conditioning and heat pump systems. For example, in the automobile air-conditioning systems, micro-scale channels with diameters of 0.6 to 1 mm are generally used in evaporators, internal heat exchangers and gas coolers while macro- and micro-channels are used for CO₂ refrigeration and heat pump systems. Due to the significant differences of two-phase flow and evaporation heat transfer phenomena in micro-scale channels as compared to conventional size channels or macro-scale channels, emphasis has been put on the characteristics of two-phase flow and heat transfer in small and micro-scale flow passages due to the rapid development of micro-scale devices in recent years [9 – 15]. Experimental studies and models on CO₂ flow boiling and two-phase flow characteristics have been conducted in both macro- and microchannels so far [17 – 24].

One very important issue should be the clarification of the distinction between micro-scale channels and macro-scale channels. However, a universal agreement is not clearly established in the literature. Instead, there are various definitions on this issue [8 – 10, 12 – 16]. Here, just to show two examples, based on engineering practice and application areas such as refrigeration industry in the

small tonnage units, compact evaporators employed in automotive, aerospace, air separation and cryogenic industries, cooling elements in the field of microelectronics and micro-electro-mechanical-systems, Kandlikar [10] defined the following ranges of hydraulic diameters D_h which are attributed to different classifications:

- Conventional channels: $D_h > 3$ mm.
- Minichannels: $D_h = 200 \mu\text{ m} - 3$ mm.
- Microchannels: $D_h = 10 \mu\text{ m} - 200 \mu\text{ m}$.

Kew and Cornwell [11] earlier proposed the Confinement number Co for the distinction of macro- and micro-scale channels, as

$$Co = \frac{1}{D_h} \sqrt{\frac{4\sigma}{g(\rho_L - \rho_G)}} \quad (1)$$

which is based on the definition of the Laplace constant [13, 16].

Other different definitions are also proposed as summarized in a recent review by Cheng and Xia [8]. However, there is no agreement on the definition of a micro-scale channel so far. Figure 4 shows the comparable definitions macro- and micro-scale channels for CO₂ according to Kandlikar [10] and the Confinement number Co [11], which shows the big difference among these criteria. In this paper, the distinction between macro- and micro-scale channels by the threshold diameter of 3 mm is adopted due to the lack of a well-established theory but is in line with those recommended by Kandlikar [10] and also for the practical use in the CO₂ air-conditioning, heat pump and refrigeration systems.

Critical analysis of experimental data of CO₂ evaporation heat transfer inside macro- and micro-channels

Quite different evaporation heat transfer and two-phase flow behaviors of CO₂ have been shown for high and low reduced pressures in the existing studies [1, 17]. The evaporation heat transfer and two-phase flow characteristics of CO₂ at the saturation temperatures ranging from 0 to 25°C show quite different characteristics as compared to those of conventional refrigerants due to the significant differences in physical properties. Generally, CO₂ has much higher evaporation heat transfer and much lower pressure drops than other low-pressure refrigerants. One feature is the dominance of the nucleate boiling at low/moderate vapor qualities prior to dryout [21 - 26]. Another feature is that the dryout in CO₂ flow boiling occurs much earlier (at relatively lower vapor qualities) than conventional refrigerants. Furthermore, the effect of the saturation temperature on the evaporation heat transfer coefficients is noticeable. At higher saturation temperatures, the nucleate boiling is more pronounced and plays an important role at the low vapor quality [17 – 19].

However, the experimental evaporation results from the different independent studies show somewhat quite different evaporation heat transfer trends at similar test conditions and thus it is difficult to understand the mechanisms and to develop relevant prediction methods. Cheng et al. [17 - 19] did comprehensive comparisons and analysis in their development of generalized mechanistic evaporation models. Figure 5 shows the two opposite evaporation heat transfer characteristics at the same saturation temperature in the studies of Pettersen [21] and Yoon et al. [25]. Heat transfer coefficients increase with increasing saturation temperature in the study of Pettersen [21] while they decrease in the study of Yoon et al. [25]. The only big difference between the two studies is the diameter of the test channels but the effect of channel size should not be so big. For another example of the channel size effect, Figure 6 shows comparative results of Yun et al. [22] in two microchannels

having two diameters of 1.53 mm and 1.54 mm at the same test conditions. Their results show that the evaporation heat transfer coefficients can be higher up to 80% with a very little change of hydraulic diameter from 1.53 mm to 1.54 mm at the same conditions. No explanation why there is such a big difference even was offered in their paper. As their study is regarding evaporation in the micro-channels, one possible reason is the issue of measurement accuracy which may be caused due to unstable and transient evaporation processes occurred in the micro-channels. This can significantly affect the prediction methods. Some detailed analysis of the evaporation mechanisms of unstable and transient evaporation processes has been presented in the relevant section of this paper. The evaporation heat transfer results of Hihara and Tanak [24] at a mass velocity of 360 kg/m²s, a saturation temperature of 15 °C and a heat flux of 18 kW/m² with two different tube diameters, 4 and 6 mm. Their evaporation heat transfer coefficients in the 4 mm channel are twice those in the 6 mm channel. In addition, the trends of the heat transfer coefficients are totally different. As both diameters are in the range of macro scale, it is surprising that the diameter has such a big effect on the heat transfer values and trends. Hence, in summary, there is still not a clear view of why CO₂ data do not conform to conventional trends and also differ widely from one study to another. It should be pointed that these experiments were conducted at high saturation temperatures which correspond to high reduced pressures. The effective results may come from the physical properties and evaporation processes in the range of close to critical point. Some physical mechanisms are still needed to explain these different evaporation processes.

Furthermore, CO₂ evaporation processes at low temperatures are important in refrigeration systems. There are several studies of CO₂ at low temperatures in the literature but still very limited information available. For example, Bredensen et al. [27] performed the boiling heat transfer experiments with CO₂ at temperatures of -10°C and -25°C. The experimental results show the heat

transfer coefficient increases with vapor quality until dryout, which is opposite to the trend of their data at 0°C. Knudsen and Jensen [28] measured flow boiling heat transfer coefficients of CO₂ in a horizontal tube of diameter 10.06 mm at the saturation temperatures of -28°C and -30°C. Their boiling heat transfer coefficients are much lower than others' data. Zhao and Bansal [29] presented experimental evaporation heat transfer data at -30°C. Park and Hrnjak [30] showed the heat transfer coefficients in a 6.1 mm inner diameter tube at -30 and -15 °C for various mass fluxes and heat fluxes. It is difficult to explain the experimental results in some studies at low temperatures.

According to the analysis of the existing experimental evaporation heat transfer results in both macro- and micro-channels at both high and low saturation temperatures in the literature. There are very big differences among these experimental results. It is difficult to explain why there are such big differences for the similar test conditions. Therefore, it is recommended that more and accurate experimental results are needed by carefully designed experiments on CO₂ evaporation heat transfer. In the aspect of prediction methods, the available empirical evaporation heat transfer methods do not capture the parametric trends in dryout and mist flow regimes and cannot explain the physical mechanisms although they predict some data well in some cases [1, 17 – 19]. Therefore, an accurate heat transfer model based on flow regimes for CO₂ evaporation in macro- and micro-channels is needed for both low and high saturation temperature and a wide range of operation conditions, but first accurate experimental evaporation results in both macro- and micro-channel under wide test conditions are needed.

Regarding the CO₂ evaporation heat transfer mechanisms, high reduced pressures and low surface tensions for CO₂ compared to conventional refrigerants have a significant effect on both nucleate boiling and convection evaporation heat transfer trends. The available studies have suggested a clear dominance of nucleate boiling heat transfer even at a very large mass flux.

Therefore, CO₂ has much higher heat transfer coefficients than those of conventional refrigerants at the same saturation temperature. The available evaporation heat transfer correlations are not applicable to CO₂ evaporation and generally underpredict the experimental results of CO₂. In addition, the existing experimental studies have demonstrated that dryout trends occur earlier at moderate vapor qualities in CO₂ evaporation processes, particularly at high mass flux and high temperature conditions. In the meantime, the flow regime transitions also vary and the conventional flow pattern maps do not capture the CO₂ flow patterns. This means the CO₂ evaporation heat transfer mechanisms are different from those of evaporation of refrigerants

From the physical properties at low temperatures, it seems that these heat transfer behaviors should be similar to those at high saturation temperatures but they are not indeed. The available CO₂ evaporation heat transfer results at low temperatures cannot be explained according to the nucleate boiling dominant mechanism. Thus, understanding of the two-phase flow structures and evaporation heat transfer characteristics of CO₂ at low temperatures is also needed.

For CO₂ evaporation heat transfer in enhanced tubes, Koyama et al. [31] conducted experiments on flow boiling in a smooth copper tube and in a micro-fin copper tube at 5.3°C. From their results, the evaporation heat transfer coefficients are only slightly higher than those in the microfin tubes with a slight pressure drop increase as well. In this case, microfin tubes are not appropriate for CO₂. Cho and Kim [32] conducted experimental studies of CO₂ evaporation in micro-channels and their results show that the average evaporation heat transfer coefficients were 150 to 210 % higher than those of smooth tubes. The increase of pressure drop was much lower than the heat transfer increase. So far, only limited studies of CO₂ flow boiling in micro-fin tubes are available. Whether they significantly enhance CO₂ flow boiling heat transfer or not is still unclear due to the lack of such information. Further extensive experimental investigation is thus needed for evaporation

processes in enhanced channels. Heat transfer coefficients and the corresponding flow patterns should be observed simultaneously to understand the phenomena and mechanisms.

According to the comprehensive analysis and comparisons of the available studies [1, 17 – 19], none of the available evaporation heat transfer prediction methods was able to accurately predict the experimental results of CO₂. In particular, these empirical correlations have no information of flow patterns and do not capture the evaporation heat transfer trends. Therefore, a comprehensive flow pattern map and mechanistic evaporation heat transfer models based on flow patterns are needed for CO₂ evaporation processes and evaporator design.

A comprehensive CO₂ flow pattern map and a mechanistic CO₂ evaporation heat transfer model based on flow patterns

A proper CO₂ evaporation heat transfer model should be a mechanics one which includes the effects of CO₂ on nucleate boiling and the annular to dryout and dryout to mist flow transitions in order to accurately predict heat transfer coefficients at moderate/high vapor qualities. To this end, Cheng et al. [17, 18] proposed a new flow pattern map and a new evaporation heat transfer model based on the flow patterns specially for CO₂ evaporating inside horizontal tubes. The flow pattern map and flow pattern based mechanistic heat transfer model were developed by modifying the methods of Wojtan et al. [33, 34] which is an updated version of the Kattan et al. [35 – 37] flow pattern map and evaporation heat transfer model. In particular, Cheng et al. [17 - 20] related the flow patterns to the corresponding CO₂ evaporation heat transfer mechanisms for both macro- and micro-channels under a wide range of reduced pressures and operation conditions. Thus, their models are different from the numerous empirical models, such as the correlations of Chen [38], which do not include flow pattern information. In fact, some of these correlations predicted the data well to some extent but fail to capture the parametric trends, or ignore the dryout and mist flow regimes which are

typical working conditions for CO₂ evaporating in horizontal channels. The Cheng et al. [17, 18] model reasonably predicts the database and it covers channel diameters found in most CO₂ evaporation applications. However, their model is limited by its parameter ranges from being applicable to some important applications, for example, the mass velocity ranges from 50 to 1500 kg/m²s in CO₂ automobile air conditioning systems and other thermal systems. In addition, the heat fluxes in some applications go beyond the maximum value in the Cheng et al. [17, 18] evaporation heat transfer model. Furthermore, the model does not extrapolate well to these conditions. In addition, the heat transfer model does not include heat transfer methods for CO₂ in mist flow and bubbly flow regimes due to the lack of the experimental data in these regimes, which were not available at that time. Therefore, Cheng et al. [19, 20] updated their CO₂ evaporation heat transfer model for CO₂ to cover a wider range of conditions and these flow regimes and an updated version of the Cheng et al. evaporation model was developed. Over the past decade, their comprehensive CO₂ flow pattern map and generalized mechanistic CO₂ evaporation heat transfer model based on the flow patterns have been proved to best prediction methods by numerous researchers. In this section, the updated Cheng et al. [19, 20] CO₂ flow pattern map and evaporation heat transfer model are briefly presented and analyzed. Some simulations are also presented to show the effect of the channel size effect on the heat transfer behaviors.

The Cheng et al. [17, 19] flow pattern map for CO₂ evaporation in macro- and micro-channels

Flow patterns are very important in understanding the very complex heat transfer phenomena and mechanisms in evaporation processes inside both macro- and micro-channels [8, 9, 12 – 20]. In particular, for evaporation mechanisms in microchannels, flow regimes and bubble behaviors are the fundamentals to understanding the corresponding heat transfer and dryout phenomena. To predict the local flow patterns in a channel, a flow pattern map is used [16, 39 - 41]. Over the past decades,

successful flow pattern based evaporation heat transfer and two-phase frictional pressure drop models [33 – 37, 42 – 46] have been developed for various fluids in order to accurately predict the evaporation heat transfer coefficients. Many flow pattern maps have been developed to predict two-phase flow patterns inside channels [14 -16]. However, most flow maps were developed for adiabatic conditions and then extrapolated by users to diabatic conditions, thereby creating big discrepancies [40 – 42]. Furthermore, the existing conventional evaporation heat transfer correlations do not include any flow pattern information and generally do not capture the heat transfer trends in dryout and mist flow regimes [47]. For this reason, a number of diabatic flow pattern maps related to the corresponding evaporation heat transfer mechanisms have been developed [33 – 37, 42 - 46]. However, none of these is applicable to CO₂ evaporation in horizontal tubes because the two-phase flow characteristics of CO₂ evaporation are greatly affected by the quite different physical properties at a wide range of reduced pressures of CO₂. For example, at very high reduced pressures, surface tensions of CO₂ are quite low and thus make the bubble easily generate in the evaporation processes. Both the two phase flow patterns and evaporation heat transfer mechanisms are quite different from those at low reduced pressures and other working fluids.

Cheng et al. [19, 20] proposed a new flow pattern map and a new generalized evaporation heat transfer model specially for CO₂ in macro- and micro-channels to meet the wide range of parameters used in engineering practical applications. The physical properties of CO₂ obtained from REFPROP version 6.01 of NIST [48] were used in their flow map and heat transfer models. The CO₂ flow pattern map is intrinsically related to the evaporation heat transfer model. For non-circular channels, equivalent diameters rather than hydraulic diameters were used in the flow pattern map [17 – 20, 42, 43] as

$$D_{eq} = \sqrt{\frac{4A}{\pi}} \quad (2)$$

Using the equivalent diameter gives the same mass velocity as in the non-circular channel and thus correctly reflects the mean liquid and vapor velocities, something using hydraulic diameter in a two-phase flow does not. In the Cheng et al. [19] updated CO₂ flow pattern map, several new features were developed as compared to the Cheng et al. flow pattern map [17]:

- (1) Combining with the updated evaporation heat transfer model for CO₂, the annular flow to dryout region transition boundary was further modified so as to better fit the sharp changes in evaporation heat transfer characteristics for higher mass velocities;
- (2) Based on experimental heat transfer data, a new criterion for the dryout region to mist flow transition was proposed;
- (3) Bubbly flow occurs at very high mass velocities and very low vapor qualities and a bubbly flow pattern boundary was integrated into the map to make it more complete.

The intermittent to annular flow transition boundary is calculated with the Cheng et al. criterion [17, 19]:

$$x_{IA} = \left[1.8^{1/0.875} \left(\frac{\rho_V}{\rho_L} \right)^{-1/1.75} \left(\frac{\mu_L}{\mu_V} \right)^{-1/7} + 1 \right]^{-1} \quad (3)$$

Then, the transition boundary is extended down to its intersection with G_{strat} [17, 19]:

$$G_{strat} = \left[\frac{226.3^2 A_{LD} A_{VD}^2 \rho_V (\rho_L - \rho_V) \mu_L g}{x^2 (1-x) \pi^3} \right]^{1/3} \quad (4)$$

$$A_{LD} = \frac{A(1-\varepsilon)}{D_{eq}^2} \quad (5)$$

$$A_{VD} = \frac{A\varepsilon}{D_{eq}^2} \quad (6)$$

The annular flow to dryout region transition boundary is calculated with the new modified criterion of Wojtan et al. [33] based of the dryout data of CO₂:

$$G_{dryout} = \left\{ \frac{1}{0.236} \left[\ln \left(\frac{0.58}{x} \right) + 0.52 \right] \left(\frac{D_{eq}}{\rho_V \sigma} \right)^{-0.17} \left[\frac{1}{g D_{eq} \rho_V (\rho_L - \rho_V)} \right]^{-0.17} \left(\frac{\rho_V}{\rho_L} \right)^{-0.25} \left(\frac{q}{q_{crit}} \right)^{-0.27} \right\}^{1.471} \quad (7)$$

which is extracted from the new dryout inception equation by Cheng et al. [17]:

$$x_{di} = 0.58 e^{\left[0.52 - 0.236 We_V^{0.17} Fr_{V,Mori}^{0.17} (\rho_V / \rho_L)^{0.25} (q / q_{crit})^{0.27} \right]} \quad (8)$$

The vapor Weber number We_V and the vapor Froude number $Fr_{V,Mori}$ defined by Mori et al. [49] are calculated as

$$We_V = \frac{G^2 D_{eq}}{\rho_V \sigma} \quad (9)$$

$$Fr_{V,Mori} = \frac{G^2}{\rho_V (\rho_L - \rho_V) g D_{eq}} \quad (10)$$

and the critical heat flux q_{crit} is calculated with the Kutateladze [50] correlation as

$$q_{crit} = 0.131 \rho_V^{0.5} h_{LV} \left[g \sigma (\rho_L - \rho_V) \right]^{0.25} \quad (11)$$

The dryout region to mist flow transition boundary is calculated with the new criterion developed in this study based on the dryout completion data for CO₂:

$$G_M = \left\{ \frac{1}{0.502} \left[\ln \left(\frac{0.61}{x} \right) + 0.57 \right] \left(\frac{D_{eq}}{\rho_V \sigma} \right)^{-0.16} \left[\frac{1}{g D_{eq} \rho_V (\rho_L - \rho_V)} \right]^{-0.15} \left(\frac{\rho_V}{\rho_L} \right)^{0.09} \left(\frac{q}{q_{crit}} \right)^{-0.72} \right\}^{1.613} \quad (12)$$

which is extracted from the dryout completion (which means the wall remains completely dry) equation developed in this study by solving for G_M from the dryout completion equation by Cheng et al. [17]:

$$x_{de} = 0.61e^{\left[0.57 - 0.502We_V^{0.16} Fr_{V,Mori}^{0.15} (\rho_V / \rho_L)^{-0.09} (q / q_{crit})^{0.72}\right]} \quad (13)$$

The intermittent to bubbly flow transition boundary is calculated with the criterion which arises at very high mass velocities and low qualities [35 -37]:

$$G_B = \left\{ \frac{256 A_{VD} A_{LD}^2 D_{eq}^{1.25} \rho_L (\rho_L - \rho_V) g}{0.3164 (1-x)^{1.75} \pi^2 P_{iD} \mu_L^{0.25}} \right\}^{1/1.75} \quad (14)$$

The updated CO₂ flow pattern map was compared to the observations of Gashe [51] for CO₂ evaporation inside a 0.8 mm diameter rectangular channel for various mass velocities. The map correctly predicts 82% of the total 28 flow patterns of Gashe. Over the past years, the CO₂ flow map has been widely used in identify flow regimes inside channels including enhanced tubes and properly identified the flow patterns of CO₂ [52 - 54].

The Cheng et al. [17 – 20] mechanistic heat transfer model for CO₂ evaporation in macro- and micro-channels

An updated generalized CO₂ evaporation heat transfer model was developed by modifying the Cheng et a. [17, 18] evaporation heat transfer model [19, 20]. By incorporating the updated new CO₂ flow pattern map, the new updated heat transfer model is physically related to the flow regimes of CO₂ evaporation, and thus correspondingly the new model has been extended to a wider range of conditions and to include new heat transfer calculation methods in mist flow and bubbly flow regimes. The new generalized flow boiling heat transfer model predicted reasonably well an extensive experimental database derived from the literature [19, 20].

To develop a generalized CO₂ evaporation heat transfer model, it is essential that the model is not only numerically accurate but that it also correctly captures the heat transfer trends in the data to be useful for heat exchanger design and optimization. Most importantly, the evaporation heat transfer mechanisms should be related to the corresponding flow patterns and can be physically explained according to flow pattern transitions. Several new modifications were implemented in the updated generalized evaporation heat transfer model for CO₂. It should be pointed out that changes to the flow pattern map also have an effect on the evaporation heat transfer model: the new dryout inception vapor quality correlation Eq. (8) and a new dryout completion vapor quality correlation Eq. (13) are used to better segregate the data into these regimes, which have sharply different heat transfer performances. Accordingly, the evaporation heat transfer correlation in the dryout region was updated. In addition, a new mist flow heat transfer correlation for CO₂ was developed based on the CO₂ data and a heat transfer method for bubbly flow was adopted for completeness sake. With these modifications, the new generalized evaporation heat transfer model for CO₂ was developed to meet a wider range of conditions and to cover all flow regimes [19, 20].

The generalized equation for the local flow boiling heat transfer coefficients h_{tp} in a horizontal tube is expressed as:

$$h_{tp} = \frac{\theta_{dry} h_V + (2\pi - \theta_{dry}) h_{wet}}{2\pi} \quad (15)$$

where θ_{dry} is the dry angle defined in Fig. 7. The dry angle θ_{dry} defines the flow structures and the ratio of the tube perimeter in contact with liquid and vapor. In stratified flow, θ_{dry} equals the stratified angle θ_{strat} which can be found in [17, 34, 37]. In annular (A), intermittent (I) and bubbly (B) flows, $\theta_{dry} = 0$. For stratified-wavy flow, θ_{dry} varies from zero up to its maximum value θ_{strat} . Stratified-wavy flow has been subdivided into three subzones (slug, slug/stratified-wavy and stratified-wavy)

to determine θ_{dry} . The vapor phase heat transfer coefficient on the dry perimeter h_V is calculated with the Dittus-Boelter [55] correlation assuming tubular flow in the tube.

The heat transfer coefficient on the wet perimeter h_{wet} is calculated with an asymptotic model that combines the nucleate boiling and convective evaporation heat transfer contributions to evaporation heat transfer by the third power:

$$h_{wet} = \left[(Sh_{nb})^3 + h_{cb}^3 \right]^{1/3} \quad (16)$$

where h_{nb} , S and h_{cb} are respectively nucleate boiling heat transfer coefficient, nucleate boiling heat transfer suppression factor and convective evaporation heat transfer coefficient. The nucleate boiling heat transfer coefficient h_{nb} is calculated with the Cheng et al. [17] nucleate boiling correlation for CO₂ which is a modification of the Cooper [56] correlation:

$$h_{nb} = 131 p_r^{-0.0063} (-\log_{10} p_r)^{-0.55} M^{-0.5} q^{0.58} \quad (17)$$

The Cheng et al. [17] nucleate boiling heat transfer suppression factor S for CO₂ is applied to reduce the nucleate boiling heat transfer contribution due to the thinning of the annular liquid film:

$$\text{If } x < x_{IA}, S = 1 \quad (18)$$

$$\text{If } x \geq x_{IA}, S = 1 - 1.14 \left(\frac{D_{eq}}{0.00753} \right)^2 \left(1 - \frac{\delta}{\delta_{IA}} \right)^{2.2} \quad (19)$$

Furthermore, if $D_{eq} > 7.53 \text{ mm}$, then set $D_{eq} = 7.53 \text{ mm}$. The liquid film thickness δ shown in Fig. 7 is calculated with the expression proposed by El Hajal et al. [45]:

The convective evaporation heat transfer coefficient h_{cb} is calculated with the following correlation assuming an annular liquid film flow from the original model [37]:

$$h_{cb} = 0.0133 \text{Re}_\delta^{0.69} \text{Pr}_L^{0.4} \frac{k_L}{\delta} \quad (20)$$

where liquid film Reynolds number Re_{δ} is the range of 199 to 20399 and liquid Prandtl number Pr_L is in the range of 3.14 to 5.47 in the original model.

Heat transfer coefficient in the dryout region is calculated by a linear interpolation [17]. A heat transfer model for bubbly flow was added to the model for completeness sake. The heat transfer coefficients in bubbly flow regime are calculated by the same method as that in the intermittent flow. Eq. (9) is used to calculate the local evaporation heat transfer coefficients. In bubbly (B) flow, the dryout angle $\theta_{dry} = 0$.

The updated generalized evaporation heat transfer model was compared to an extensive database [20]. The updated generalized heat transfer model was compared to an experimental database containing 1124 data points. Good agreement between the predicted and experimental data was found in general with 71.4% of the entire database and 83.2% of the database without the dryout and mist flow data predicted within $\pm 30\%$. The predictions for the dryout and mist flow regions were less satisfactory due to the limited number of data points, the higher inaccuracy in such data, scatter in some data sets ranging up to 40%, significant discrepancies from one experimental study to another and the difficulties associated with predicting the inception and completion of dryout around the perimeter of the horizontal tubes. Just to show one example here, Figure 8(a) shows the comparison of the predicted evaporation heat transfer coefficients to the experimental data of Yun et al. [26] and Figure 8(b) shows the corresponding flow map. The model does not only capture the heat transfer trend but also predicts 85.7% of the data of Yun et al. [26] within $\pm 30\%$. However, as it is harder to predict (and harder to accurately measure) heat transfer data in the dryout and mist flow regimes, the updated general heat transfer model does not always predict the experimental data in these two flow regimes satisfactorily. Therefore, further improvement in the measurements of heat transfer in these flow regimes are needed.

Overall, the updated generalized evaporation heat transfer model predicts the overall database quite well. However, for the dryout and mist flow regimes with partially or all dry perimeters, the heat transfer model is only partially satisfactory. For these last two regimes, many of the experimental data sets have a level of scatter ranging up to 40% themselves. In part, the larger errors are due to the very sharp change in trend in these data with vapor quality, where an error of a 2-3% in vapor quality in the energy balance of the experiments or in the prediction of x_{di} and/or x_{de} immediately results in a heat transfer prediction error of 50%. Another possible reason for the low prediction in these two flow regimes is the effect of unstable evaporation and transient heat transfer in these two flow regimes, which are not well understood and incorporated in the flow map and heat transfer model. Therefore, more careful experiments are needed in these two regimes to provide more accurate heat transfer data, with attention to also determine the transitions x_{di} and x_{de} , because they are typical working conditions in the micro-scale channels of extruded multi-port aluminum tubes used for automobile air-conditioners that operate over a wide range of mass velocities up to as high as 1500 kg/m²s. Furthermore, physical mechanisms of unstable evaporation and transient heat transfer should be considered for improvement of the flow pattern identification and heat transfer prediction.

To understand the effect of the channel size on the CO₂ evaporation processes, simulated results for two channels with diameters of 1.15 mm and 3 mm using the model show different heat transfer trends and dryout incipience as in Figs. 9(a) and (b). Figure 9 shows the simulations of the updated flow pattern map and flow boiling model for CO₂ at the indicated conditions, superimposed on the same graphs. The process path for the vapor quality variation from $x = 0.01$ to $x = 0.99$ is shown as the horizontal broken line (dash-dot line) while the variation in the heat transfer coefficient as it changes vapor quality and flow pattern is depicted by the dashed line. The flow pattern boundaries are in solid lines. The line (dash line with arrows) indicates the calculated heat transfer coefficient at the indicated mass velocity and vapor quality. Notice the various changes in trends in the heat transfer coefficient

as this occurs. For example, when the flow regime passes from annular flow into the dryout regime, there is a sharp inflection in the heat transfer coefficient as the top perimeter of the tube becomes dry. A number of existing studies have confirmed that the Cheng et al. [17 – 20] CO₂ flow boiling heat transfer model has favorably predicted their experimental data [57 – 60]. The prediction of flow boiling heat transfer is a big challenge depending on the various fluids and conditions [47]. In particular, the microchannel effects become significant and need to be well understood [61, 62]. In particular, the evaporation mechanisms at macro- and micro-channels should be further investigated from new mechanisms relevant to unstable evaporation processes and transient heat transfer. Some initial such mechanisms are discussed in the following section.

Evaporation heat transfer mechanisms related to unstable and transient flow regimes and heat transfer phenomena

In order to better understand the evaporation phenomena and further develop accurate heat transfer prediction methods, it is essential to analyze the evaporation processes according to new heat transfer mechanisms from the standpoint of unstable and transient evaporation heat transfer, particularly according to most recent research findings in micro-channels.

Evaporation heat transfer mechanisms in channels

Evaporation heat transfer in conventional channels is governed by two basic mechanisms of nucleate boiling dominant mechanism relating to the formation of vapor bubbles at the tube wall surface and convection dominant mechanism relating to conduction and convection through a thin liquid film with evaporation on the channel wall and at the liquid–vapor interface. The evaporation heat transfer and dryout mechanisms are intrinsically related to the bubble dynamics and flow pattern behaviors [63 - 65]. The gravity becomes important for flow boiling in horizontal conventional

channels and affects the flow patterns and heat transfer behavior. The evaporation heat transfer is strongly dependent on the heat flux in nucleation dominant boiling while the heat transfer is less dependent on the heat flux and strongly dependent on the mass flux and vapor quality in convection dominant evaporation. One may assume that these mechanisms function independently of one another for simplicity. However, the two main mechanisms may actually coexist at high vapor qualities, where the convective evaporation gradually suppresses the nucleate boiling [8]. Therefore, the nucleate boiling and convective evaporation contributions to the heat transfer process can be superimposed by very complex mechanisms which are not yet fully understood so far. In particular, for micro-channels, the evaporation heat transfer mechanisms are strongly affected by the bubble behaviors in confined space and the unstable bubble dynamics [64 – 66]. These observed phenomena have not yet incorporated in the low pattern and heat transfer prediction methods.

In general, the evaporation heat transfer mechanisms in macroscale channels have laid a good foundation to investigating the flow boiling heat transfer mechanisms in microscale channels which needs to be systematically explored through considering more affecting factors such as bubble confinement, channel size and shape effects, surface roughness, accurate liquid film and heat transfer measurement and corresponding flow regime observation with state-of-the-art experimental technique and proper data analysis methods. Furthermore, generalized prediction methods are needed for evaporation heat transfer based on the flow patterns. In this aspect, several flow pattern based evaporation heat transfer models have been developed show promising results. In particular, Cheng et al. developed the comprehensive flow pattern map and a generalized evaporation heat transfer model based on flow patterns specially for CO₂. However, further improvement of the model should focus on the dryout and mist flow regimes by incorporating new insights of mechanisms under unstable evaporation flow and transient heat transfer phenomena.

Unstable and transient evaporation heat transfer phenomena in channels

As mentioned in the foregoing, the mechanisms of the unstable and transient flow boiling heat transfer in microscale channels play a vital role in developing proper evaporation prediction methods. Evaporation heat transfer and two phase flow instability in macro-channels are divided into dynamic and static instabilities. For dynamic instability, it is related to pressure, mass flux and temperature. It is commonly recognized that three types of oscillations exist in two phase flow and evaporation processes in a macroscale channels: pressure drop oscillation, density wave oscillation and thermal oscillation. These unstable behaviors may even cause deterioration of heat transfer and thus cause dryout and boiling crisis which may occur in subcooled conditions. Furthermore, Investigation of dynamic flow boiling instability in microchannels have been extensively conducted to understand the phenomena and mechanisms [64 – 73]. Qu and Mudawar [64] observed backflow phenomena and they found that the inlet/outlet configuration may have a significant effect of the unstable flow. Wang et al. [65, 66] found fluctuation of temperature and oscillations in the microchannels which correspond to the unstable flow regime and flow regime transition. Hetsroni et al. [67] observed periodic annular flow and periodic dry steam flow in the microchannel. The unstable flow boiling phenomena are caused due to the confined flow regimes changes, back flow and non-uniform flow and so on. Huang et al. [68] conducted experimental on the thermal response of multi-microchannels during flow boiling of R236fa and R245fa under transient heat loads with flow visualization. They investigated the base temperature response of multi-microchannel evaporators under transient heat loads, including cold startups and periodic step variations in heat flux using two different test sections for a wide variety of flow conditions. For cold startups, it was found that reducing the inlet orifice width, heat flux magnitude, inlet subcooling, and outlet saturation temperature but increasing the mass flux decreased the maximum base temperature. In the meanwhile, the time required to initiate boiling increased with the inlet orifice width, mass flux, inlet

subcooling, and outlet saturation temperature but decreased with the heat flux magnitude. For periodic variations in heat flux, the resulting base temperature was found to oscillate and then damp out along the flow direction. Furthermore, the effects of mass flux and heat flux pulsation period were insignificant. Furthermore, the onset of flow boiling occurred earlier for higher heat flux magnitude. Recently, Xia et al. [71] conducted experimental study and dynamic simulation of continuous two-phase instable boiling in parallel multiple micro-channels. They found that the backflow causes instability of the liquid and the two-phase interface and therefore changes the thermal resistances of fluid. Furthermore, they developed a dynamic simulation model using the thermal network method and conducted dynamic simulations using the model. They found that the axial thermal conduction in the channel walls generates a negative differential zone in the heat power characteristic curves, where the wall temperature drops with increasing the heat flux in the negative differential zone. The main operational parameters of the boiling process can keep it stable at this state, or the boiling begins to oscillate from this state. The average fluid temperature at the stable and the instable boiling is shown in Fig. 10 (a) and the wall temperature difference between the subcooled region and saturated region at stable state are shown in Fig. 10 (b). The fluid and wall temperature fluctuations may cause big errors when prediction the evaporation heat transfer coefficients using the existing prediction methods. So far, unstable and transient evaporation heat transfer in microchannels, as a special important topic, has not yet been well understood. Therefore, systematic experimental, analytical and modelling studies of the unstable and transient evaporation processes in microchannels are needed.

Application of the Cheng et al. [17 – 20] CO₂ evaporation model in engineering design and simulation of evaporators in CO₂ thermal systems

The Cheng et al. evaporation heat transfer model has been widely used for simulations of CO₂ refrigeration, air-conditioning and heat pump systems by a number of researchers [74 – 79]. For example, in order to improve the system performance of the CO₂ heat pump, it is necessary to develop an optimum design and a control method for the CO₂ heat pump water heater. Yamaguchi et al. [76] have developed a high-precision and general-purpose system simulation model for the CO₂ heat pump water heater and investigated the validity of the model with detailed experiments. Figure 11 shows the system flow diagram of the CO₂ heat pump water heater in their study. This system consists of a gas cooler, an evaporator, an internal heat exchanger, a compressor, and an expansion valve. In the internal heat exchanger, the refrigerant from the evaporator cools the refrigerant that flows in from the gas cooler, and then flows into the compressor, where its pressure and temperature are increased. The heated refrigerant then flows into the gas cooler, where it heats up the supplied water. Subsequently, it flows into the internal heat exchanger and is expanded by the expansion valve. Finally, the refrigerant flows into the evaporator. In the evaporator, the refrigerant absorbs heat from the ambient air, after which it flows back to the internal heat exchanger. In this system, a cross-finned tube heat exchanger with smooth plate fins is adapted for use in the evaporator in the heat pump system as shown in Fig. 12. In the development of their model, the local heat transfer coefficient and two phase flow frictional pressure drop inside the tubes are calculated using the Cheng et al. flow pattern based evaporation heat transfer model [19, 20]. The models were developed specifically for CO₂ to predict the evaporation heat transfer coefficient and the two phase frictional pressure drop on the basis of the flow pattern map for CO₂. Yamaguchi et al. [76] compared the predicted and measured heat transfer rates and COPs and confirmed that the predicted results are in good agreement with the measured values. For the evaporator, the results show good agreement between the measured and predicted heat transfer rate as shown in Fig. 13. This means that the Cheng et al. [19, 20] models

work well for the evaporator in their study. The maximum difference between the predicted and measured COP is 5.4%, and the average difference is 0.9% as shown in Fig. 13.

Considering the actual heat transfer processes of heat exchangers and characteristics of components adopted in the cycle of air-source trans-critical CO₂ heat pump water heater system, Wang et al. [77] conducted simulation for the heat pump cycle. In their simulation model, the Cheng et al. evaporation model was adopted in the evaporator model in their simulation. It shows good agreement with the experimental results. Faria et al. [78] investigated of the behavior of the solar evaporator and expansion valve assembly of a transcritical CO₂ heat pump in transient and steady conditions. The dynamic behavior of systems using CO₂ as a refrigerant is significantly influenced by the dynamics of the heat transfer mechanisms. The solar evaporator model is based on the equations of conservation of mass, momentum, and energy. The model validation is realized by comparing simulation results with the Cheng et al. models and the experimental data. The model is a useful tool for analyzing the behavior in transient and steady conditions simulating various operating conditions of the heat pump including solar radiation, ambient temperature, wind speed and atmospheric conditions. Yang et al. [79] investigated experimentally a prototype of combined R134a and transcritical CO₂ heat pump. The experimental results demonstrated that the combined system could operate reliably and supply stable temperature hot water over a wide range of ambient temperatures and feed water temperatures. The experimental results also showed that ambient temperature had a large effect on the system performance. Furthermore, they investigated the improvement of the combined system in comparison to the standard transcritical CO₂ heat pump, a simple mathematical model was developed and validated by the experimental data. The comparison results showed that the combined system could offer higher system COP at experimental ambient and feed water temperatures. In their evaporator model, the Cheng et al. models were used in the simulations. In general, the Cheng et al. flow pattern-based evaporation heat transfer and two-phase

pressure drop models show good agreement with the experimental data in the existing studies when used in modeling the evaporators in these systems.

As an excellent coolant, CO₂ may be used in electronic cooling [5], two-phase thermosyphon loop [80 - 81] and evaporative CO₂ cooling system for the upgrade of the Compact Muon Solenoid (CMS) pixel detector [54] etc. Furthermore, new applications with CO₂ in various thermal systems with microscale channel evaporators should be further explored to improve the energy efficiency and environment safe.

According to the existing studies, it has confirmed that the Cheng et al. models favorably predict the evaporation heat transfer, two phase pressure drop and flow patterns in heat exchanger tubes. This also means that the mechanistic models based on flow patterns are promising methods. Therefore, more accurate flow pattern observations and heat transfer experimental data under a wide range test conditions are still needed. Furthermore, understanding the oil effects on the two phase flow and evaporation heat transfer of CO₂ and relevant practical models are also needed [82, 83]. New thermal and energy systems should also be targeted to extend the applications of CO₂ in engineering practice.

Conclusions

Fundamentals and applications of CO₂ evaporation processes and modeling are analyzed and reviewed in this paper. The Cheng et al. generalized two-phase flow patterns and heat transfer model for CO₂ evaporation in macroscale- and microscale-channels and their applications in modeling and designing CO₂ evaporators in refrigeration, air-conditioning and heat pump systems are presented. The available experimental studies are analyzed at first. Then, the Cheng et al. two-phase flow pattern map for CO₂ evaporation and flow pattern-based evaporation heat transfer model are presented. Modeling of CO₂ evaporation and simulation/design of CO₂ evaporators are presented and analyzed.

Furthermore, evaporation heat transfer mechanisms, unstable and transient evaporation phenomena are discussed. The research needs in the future are identified according to the comprehensive review and analysis. Finally, applications of the model in CO₂ evaporator simulation and various thermal systems are presented. application. The main conclusions are summarized as follows:

- (1) According to the analysis, the available experimental results have shown different evaporation heat transfer and two-phase flow characteristics of CO₂ at high and low reduced pressures. The evaporation heat transfer and two-phase flow of CO₂ at saturation temperatures ranging from 0 to 25°C show different characteristics from those of conventional refrigerants due to the significant differences in thermal physical and transport properties. CO₂ has much higher evaporation heat transfer than other low-pressure refrigerants such as R134a and ammonia etc.
- (2) The evaporation heat transfer mechanisms are the dominance of the nucleate boiling at low/moderate vapor qualities prior to dryout and the occurrence of dryout in CO₂ at relatively lower vapor qualities than conventional refrigerants. Furthermore, the effect of the saturation temperature on the evaporation heat transfer coefficient is more noticeable. At high saturation temperatures, the nucleate boiling mechanism is more pronounced at low vapor qualities.
- (3) The experimental data from the different independent studies show somewhat different evaporation heat transfer trends at similar test conditions. It is difficult to explain the differences at similar conditions or the parameter effects on the evaporation heat transfer behaviors according to the physical mechanisms. This might be caused by large measurement uncertainties. Therefore, more accurate experimental data are needed for CO₂ evaporation in both macro- and micro-channels through well designed test facilities and

careful experiments. In particular, a wide range of test conditions should be designed to meet the practical needs in industry.

- (4) Overall, the Cheng et al. [17 – 20] flow pattern map and flow pattern based evaporation heat transfer model for CO₂ reasonably predicts the observed flow patterns and experimental heat transfer coefficients in the literature and also capture properly the parametric trends. However, for the dryout and mist flow regimes with partially or all dry perimeters, the heat transfer model is only partially satisfactory. Therefore, more careful experiments are needed in these two regimes to provide more accurate heat transfer data, with attention to also determine the transitions of dryout incipience and dryout completions.
- (5) New mechanisms should be investigated to understand the unstable and transient evaporation processes. Furthermore, effort should be made to develop new prediction methods by considering the unstable and transient two phase flow and evaporation mechanisms.
- (6) The Cheng et al. [17 -20] flow pattern based CO₂ evaporation heat transfer model have been used to simulate the evaporators in various thermal systems by a number of researchers. It shows that the experimental results favorably agree with the simulations results. Therefore, it is recommended that Cheng et al. methods be used in the design and simulation of CO₂ evaporators.
- (7) As an excellent working fluid, CO₂ has also been investigated in other practical applications such as electronic chips cooling, evaporative CO₂ cooling system for the upgrade of the CMS pixel detector and potential for renewable energy and power generation. Therefore, effort should be made to explore new applications of CO₂ evaporation in the relevant fields.

Acknowledgement

This research is supported by the Science and Technology Project of Beijing Education Committee (No. KZ201810005006).

Nomenclature

A	cross-sectional area of flow channel, m^2 ; annular flow regime
A_{LD}	liquid dimensionless cross-sectional area
A_{VD}	vapor dimensionless cross-sectional area
B	bubbly flow regime
Co	Confinement number, defined by Eq. (1)
COP	coefficient of performance
c_p	specific heat, J/kgK
D	internal tube diameter, m; dryout flow regime
d_i	inner tube diameter of fin-tube evaporator, m
E	power consumption, kW
Fr_L	liquid Froude number, $G^2/(\rho_L^2 g D_{eq})$
$Fr_{V,Mori}$	vapor Froude number, $G^2/(\rho_v(\rho_L - \rho_v)g D_{eq})$ defined by Mori et al. [49]
G	total vapor and liquid two-phase mass flux, kg/m^2s
g	gravitational acceleration, $9.81 m/s^2$
h	heat transfer coefficient, W/m^2K
h_{LV}	latent heat of vaporization, J/kg
I	intermittent flow regime
i	enthalpy, kJ/kg

k	thermal conductivity, W/mK
L_d	distance of tubes, m
L_f	dimension of fin, m
L_p	pitch of tubes, m
L_t	tube length between two fins, m
M	molecular weight, kg/kmol; mist flow regime
P_{iD}	dimensionless perimeter of interface
Pr	Prandtl number, $c_p\mu/k$
p	pressure, Pa
p_r	reduced pressure, p/p_{crit}
Q	heat exchanger flow rate, kW
q	heat flux, W/m ²
Re_δ	liquid film Reynolds number, $4G(1-x)\delta/(\mu_L(1-\varepsilon))$
S	nucleate boiling suppression factor
T	temperature, K
t	time, s
SW	stratified-wave flow regime
We_v	vapor Weber number, $G^2D_{eq}/(\rho_v\sigma)$
x	vapor quality

Greek symbols

ε	void fraction
ΔT	temperature difference between fluid and tube wall, K

δ	liquid film thickness, m
μ	dynamic viscosity, Ns/m ²
θ_{dry}	dry angle of tube perimeter, rad
ρ	density, kg/m ³
σ	surface tension, N/m

Subscripts

<i>cb</i>	convective boiling
<i>crit</i>	critical
<i>D</i>	dimensionless
<i>d</i>	distance
<i>de</i>	dryout completion
<i>di</i>	dryout inception
<i>eff</i>	effective
<i>eq</i>	equivalent
<i>f</i>	fluid, fin
<i>G</i>	gas
<i>h</i>	hydraulic
<i>I</i>	intermittent flow
<i>IA</i>	intermittent flow to annular flow transition
<i>i</i>	inner
<i>in</i>	inlet
<i>L</i>	liquid

<i>M</i>	mist flow
<i>nb</i>	nucleate boiling
<i>p</i>	pitch
<i>sat</i>	saturation
<i>strat</i>	stratified
<i>t</i>	tube
<i>tp</i>	two-phase
<i>V</i>	vapour
<i>wet</i>	wet perimeter
<i>wi</i>	inlet water
δ	liquid film thickness

References

1. J. R. Thome, and G. Ribatski, "State-of-the-art of two-phase flow and flow boiling heat transfer and pressure drop of CO₂ in macro- and micro-channels." *Int. J. Refrig.*, vol. 28, no. 8, pp. 1149-1168, 2005. DOI: 10.1016/j.ijrefrig.2005.07.005.
2. J. R. Thome, L. Cheng, G. Ribatski, and L. F. Vales, "Flow boiling of ammonia and hydrocarbons: A state-of-the-art review," *Int. J. Refrig.*, vol. 31, no. 4, pp. 603-620, 2008. DOI: 10.1016/j.ijrefrig.2007.11.010.
3. M. H. Kim, J. Pettersen, and C. W. Bullard, "Fundamental process and system design issues in CO₂ vapor compression systems," *Prog. Energy Combust. Sci.*, vol. 30, no. 2, pp. 119-174, 2000. DOI: 10.1016/j.pecs.2003.09.002.

4. L. Cheng, G. Ribatski, and J. R. Thome, "Analysis of supercritical CO₂ cooling in macro- and micro Channels," *Int. J. Refrig.*, vol. 31, no. 8, pp. 1301-1316, 2008. DOI: 10.1016/j.ijrefrig.2008.01.010.
5. L. Cheng, and J. R. Thome, "Cooling of microprocessors using flow boiling of CO₂ in micro-evaporators: Preliminary analysis and performance comparison," *Appl. Therm. Eng.*, vol. 29, no. 11 – 12, pp. 2426-2432, 2009. DOI: 10.1016/j.applthermaleng.2008.12.019.
6. L. Cheng, "Evaluation of correlations for supercritical CO₂ cooling convective heat transfer and pressure drop in macro- and micro-scale tubes," *Int. J. Microscale Nanoscale Therm. Fluid Transp. Phenom.*, vol. 5, no. 2, pp. 113-126, 2014.
7. S. Sawalha, "Using CO₂ in supermarket refrigeration," *ASHRAE J.*, vol. 47, no. 8, pp. 26-30, 2005.
8. L. Cheng, and D. Xia, "Fundamental issues, mechanisms and models of flow boiling heat transfer in microscale channels," *Int. J. Heat Mass Transfer*, vol. 108 (Part A), pp. 97-127, May, 2017. DOI: 10.1016/j.ijheatmasstransfer.2016.12.003.
9. L. Cheng, "Fundamental issues of critical heat flux phenomena during flow boiling in microscale-channels and nucleate pool boiling in confined spaces," *Heat Transfer Eng.*, vol. 34, no.13, pp. 1011-1043, 2013. DOI: doi.org/10.1080/01457632.2013.763538
10. S. G. Kandlikar, "Fundamental issues related to flow boiling in minichannels and microchannels," *Exp. Therm. Fluid Sci.*, vol. 26, no. 2 – 4, pp. 389-407, 2002. DOI: 10.1016/S0894-1777(02)00150-4.
11. P. A. Kew, and K. Cornwell, "Correlation for the prediction of boiling in small-diameter channels," *Appl. Therm. Eng.*, vol. 17, no. 8 - 10, pp. 705-715, 1997. DOI: 10.1016/S1359-4311(96)00071-3.

12. L. Cheng, D. Mewes, and A. Luke, "Boiling phenomena with surfactants and polymeric additives: A state-of-the-art review," *Int. J. Heat Mass Transfer*, vol. 50, no. 13 – 14, 2744-277, 2007. DOI: 10.1016/j.ijheatmasstransfer.2006.11.016.
13. L. Cheng, D. Mewes, "Review of two-phase flow and flow boiling of mixtures in small and mini channels," *Int. J. Multiphase Flow*, vol. 32, no. 2, pp. 183-207, 2006. DOI: 10.1016/j.ijmultiphaseflow.2005.10.001.
14. L. Cheng, Microscale Flow Patterns and Bubble Growth in Microchannels, in *Microchannel Phase Change Heat Transfer*, Editor: Sujoy Kumar Saha, Elsevier Publisher, pp. 91-140. 2016. DOI: 10.1016/B978-0-12-804318-9.00003-0.
15. L. Cheng, Flow Boiling Heat Transfer with Models in Microchannels, in *Microchannel Phase Change Heat Transfer*, Editor: Sujoy Kumar Saha, Elsevier Publisher, pp.141-191, 2016. DOI: 10.1016/B978-0-12-804318-9.00004-2.
16. L. Cheng, G. Ribatski, and J. R. Thome, "Gas-liquid two-phase flow patterns and flow pattern maps: fundamentals and applications," *ASME Appl. Mech. Rev.*, vol. 61, no. 5, 50802, 28 pages, 2008. DOI: 10.1115/1.2955990.
17. L. Cheng, G. Ribatski, L. Wojtan, and J. R. Thome, "New flow boiling heat transfer model and flow pattern map for carbon dioxide evaporating inside horizontal tubes," *Int. J. Heat Mass Transfer*, vol. 49, no. 21 – 22, pp. 4082-4094, 2006. DOI: 10.1016/j.ijheatmasstransfer.2006.04.003.
18. L. Cheng, G. Ribatski, L. Wojtan, and J. R. Thome, "Erratum to: New flow boiling heat transfer model and flow pattern map for carbon dioxide evaporating inside tubes, [Heat Mass Transfer 49 (21-22) (2006) 4082-4094]," *Int. J. Heat Mass Transfer*, vol. 50, no. 1 – 2, pp. 391, 2007. DOI: 10.1016/j.ijheatmasstransfer.2006.07.033.

19. L. Cheng, G. Ribatski, J. Moreno Quibén., and J. R. Thome, “New prediction methods for CO₂ evaporation inside tubes: Part I - A general two-phase flow pattern map and development of a phenomenological model of two-phase flow frictional pressure drop,” *Int. J. Heat Mass Transfer*, vol. 51, no. 1 - 2, pp. 111-124, 2008. DOI: 10.1016/j.ijheatmasstransfer.2012.05.044.
20. L. Cheng, G. Ribatski, and J. R. Thome, “New prediction methods for CO₂ evaporation inside tubes: Part II - A general flow boiling heat transfer model based on flow patterns,” *Int. J. Heat Mass Transfer*, vol. 51, no. 1 - 2, pp. 125 - 135, 2008. DOI: 10.1016/j.ijheatmasstransfer.2007.04.001.
21. J. Pettersen, “Flow vaporization of CO₂ in microchannel tubes,” *Exp. Therm. Fluid Sci.*, vol. 28, pp. 111-121, 2004.
22. R. Yun, Y. Kim, and M. S. Kim, “Convective boiling heat transfer characteristics of CO₂ in microchannels,” *Int. J. Heat Mass Transfer*, vol. 48, no. 2, pp. 235-242, 2005. DOI: 10.1016/j.ijheatmasstransfer.2004.08.019.
23. R. Yun, Y. Kim, M. S. Kim, and Y. Choi, “Boiling heat transfer and dryout phenomenon of CO₂ in a horizontal smooth tube,” *Int. J. Heat Mass Transfer*, vol. 46, no. 13, pp. 2353-2361, 2003. DOI: 10.1016/S0017-9310(02)00540-9.
24. E. Hihara, and S. Tanaka, “Boiling heat transfer of carbon dioxide in horizontal tubes,” In: *Preliminary Proc. IIR Gustav Lorentzen Conf. Natural Working Fluids*, Purdue, pp. 279-284, 2000.
25. S. H. Yoon et al., “Characteristics of evaporative heat transfer and pressure drop of carbon dioxide and correlation development,” *Int. J. Refrig.*, vol. 27, no. 2, pp. 111-119, 2004. DOI: 10.1016/j.ijrefrig.2003.08.006.

26. R. Yun, Y. Kim, and M. S. Kim, "Flow boiling heat transfer of carbon dioxide in horizontal mini tubes," *Int. J. Heat Fluid Flow*, v.ol. 26, no. 5, pp. 801-809, 2005. DOI: 10.1016/j.ijheatfluidflow.2005.01.004.
27. A. Bredesen, A. Hafner, J. Pettersen, P. Neksa, and K. Aflekt, "Heat transfer and pressure drop for in-tube evaporation of CO₂," In: *Proc. the Int. Conf. Heat Transfer Issues Natural Refrigerants*, University of Maryland, USA, pp. 1-15, 1997.
28. H. J. Knudsen, and R. H. Jensen, "Heat transfer coefficient for boiling carbon dioxide," In: *Workshop Proc.- CO₂ Technol. Refrigeration, Heat Pumps Air Conditioning Sys.*, Trondheim, Norway, pp. 319-328, 1997.
29. X. Zhao, and P. K. Bansal, "Flow boiling heat transfer characteristics of CO₂ at low temperatures," *Int. J. Refrig.*, vol. 30, no. 6, pp. 937-945, 2007. DOI: 10.1016/j.ijrefrig.2007.02.010.
30. C. Y. Park, and P. S. Hrnjak, "Flow boiling heat transfer of CO₂ at low temperatures in a horizontal smooth tube," *J. Heat Transfer*, vol. 127, no. 12, 1305-1312, 2005. DOI: 10.1115/1.2098853.
31. S. Koyama, S. Lee, D. Ito, K. Kuwahara, and H. Ogawa, "Experimental study on flow boiling of pure CO₂ and CO₂-oil mixtures inside horizontal smooth and micro-fin copper tubes," In: *Proc. 6th IIT-Gustav Lorentzen Conf.*, Glasgow, UK, 2004.
32. J. M. Cho, and M. S. Kim, "Experimental studies on the evaporative heat transfer and pressure drop of CO₂ in smooth and micro-fin tubes of the diameters of 5 and 9.52 mm," *Int. J. Refrig.*, vol. 30, no. 6, pp. 986-994, 2007. DOI: 10.1016/j.ijrefrig.2007.01.007.
33. L. Wojtan, T. Ursenbacher, and J. R. Thome, "Investigation of flow boiling in horizontal tubes: Part I – A new diabatic two-phase flow pattern map," *Int. J. Heat Mass and Transfer*, vol. 48, no. 14, pp. 2955-2969, 2005. DOI: 10.1016/j.ijheatmasstransfer.2004.12.012.

34. L. Wojtan, T. Ursenbacher, and J. R. Thome, "Investigation of flow boiling in horizontal tubes: Part II – Development of a new heat transfer model for stratified-wavy, dryout and mist flow regimes," *Int. J. Heat Mass and Transfer*, vol. 48, no. 14, pp. 2970-2985, 2005. DOI: 10.1016/j.ijheatmasstransfer.2004.12.013.
35. N. Kattan, J. R. Thome, and D. Favrat, "Flow boiling in horizontal tubes. Part 1: Development of a diabatic two-phase flow pattern map," *J. Heat Transfer*, vol. 120, no. 1, pp. 140-147, 1998. DOI: 10.1115/1.2830037.
36. N. Kattan, J. R. Thome, and D. Favrat, "Flow boiling in horizontal tubes: Part 2-New heat transfer data for five refrigerants," *J. Heat Transfer*, vol. 120, no. 1, pp. 148-155, 1998. DOI: 10.1115/1.2830038.
37. N. Kattan, J. R. Thome, and D. Favrat, "Flow boiling in horizontal tubes: Part-3: Development of a new heat transfer model based on flow patterns," *J. Heat Transfer*, vol. 120, no. 1, pp. 156-165, 1998. DOI: 10.1115/1.2830039.
38. J. C. Chen, "Correlation for boiling heat transfer to saturated fluids in convective flow," *Ind. Eng. Chem., Proc. Des. Dev.*, vol. 5, no. 3, pp. 322-339, 1966. DOI: 10.1021/i260019a023.
39. Y. Taitel, and A. E. Dukler, "A model for predicting flow regime transitions in horizontal and near horizontal gas-liquid flow," *AIChE J.*, vol. 22, no. 1, pp. 47-55, 1976. DOI: 10.1002/aic.690220105.
40. K. Hashitume, "Flow pattern and void fraction of refrigerant two-phase flow in a horizontal pipe," *Bull. JSME*, vol. 26, no. 219, pp. 1597-1602, 1983. DOI: 10.1299/jsme1958.26.1597.
41. D. Steiner, VDI-Wärmeatlas, Verein Deutscher Ingenieure VDI-Gesellschaft Verfahrenstechnik und Chemieingenieurwesen (GCV), Düsseldorf, Ch. Hbb, 1993.
42. J. Moreno Quibén, L. Cheng, R. J. da Silva Lima, and J. R. Thome, "Flow boiling in horizontal flattened tubes: Part I—Two-phase frictional pressure drop results and model," *Int. J. Heat Mass*

- Transfer*, vol. 52, no. 15–16, pp. 3634-3644, 2009. DOI: 10.1016/j.ijheatmasstransfer.2008.12.032.
43. J. Moreno Quibén, L. Cheng, R. J. da Silva Lima, and J. R. Thome, “Flow boiling in horizontal flattened tubes: Part II — Flow boiling heat transfer results and model,” *Int. J. Heat Mass Transfer*, vol. 52, no. 15–16, pp. 3645-3653, 2009. DOI: 10.1016/j.ijheatmasstransfer.2008.12.033.
44. J. R. Thome, and J. El Hajal, “Two-phase flow pattern map for evaporation in horizontal tubes: Latest version,” In: *1st Int. Conf. Heat Transfer, Fluid Mech.s Thermodyn.*, Kruger Park, South Africa, April 8-10, 2002, pp. 182-188.
45. J. El Hajal, J. R. Thome, and A. Cavallini, “Condensation in horizontal tubes, part 2: New heat transfer model based on flow regimes,” *Int. J. Heat Mass Transfer*, vol. 46, no. 18, pp. 3365-3387, 2003. DOI: 10.1016/S0017-9310(03)00140-6.
46. L. Cheng, G. Ribatski, and J. R. Thome, “On the Prediction of Flow Boiling Heat Transfer of CO₂,” In: *The 22nd IIR Int. Congr. Refrig.*, Beijing, P.R. China, August 21-26, 2007.
47. L. Cheng, and T. Cheng, “Comparison of six typical correlations for upward flow boiling heat transfer with kerosene in a vertical smooth tube,” *Heat Transfer Eng.*, vol. 21, no. 5, pp. 27-34, 2000. DOI: 10.1080/01457630050127928
48. REFPROP. NIST Refrigerant Properties Database 23. Gaithersburg, MD, 1998, Version 6.01.
49. H. Mori, S. Yoshida, K. Ohishi, and Y. Kokimoto, “Dryout quality and post dryout heat transfer coefficient in horizontal evaporator tubes,” In: *Proc. 3rd European Therm. Sci. Conf.*, Heidelberg, Germany, 10 – 13, September, 2000, pp. 839-844.
50. S.S. Kutateladze, “On the transition to film boiling under natural convection,” *Kotloturbostroenie*, vol. 3, 10-12. 1948.

51. J. L. Gasche, "Carbon dioxide evaporation in a single micro-channel," *J. Braz. Soc. Mech. Sci. Eng.*, vol. 28, no. 1, pp. 69-83, 2006. DOI.org/10.1590/S1678-58782006000100008.
52. L. Gao, Y. Watanabe, and T. Honda, "CO₂ Flow boiling in small diameter smooth and micro-fin tubes," *J. JSEM*, vol. 11, SS66-SS72, 2011. DOI: doi.org/10.11395/jjsem.11.s66.
53. M. Wetzel, B. Dietrich, and T. Wetzel, "Influence of oil on heat transfer and pressure drop during flow boiling of CO₂ at low temperatures," *Exp. Therm. Fluid Sci.*, vol. 59, 202-212, Nov., 2014. DOI: 10.1016/j.expthermflusci.2014.05.001.
54. J. Daguin et al. "Evaporative CO₂ cooling system for the upgrade of the CMS pixel detector at CERN," *10th IIR Gustav Lorentzen Conf. Natural Refrigerants*, Delft, The Netherlands, 30 May-1 June 2012.
55. F. W. Dittus, and L. M. K. Boelter, "Heat transfer in automobile radiator of the tubular type," *Univ. Calif. Publ. Eng.*, vol. 2, no. 13, pp. 443-461, 1930.
56. M. G. Cooper, "Saturation nucleate pool boiling: a simple correlation," *Inst. Chem. Eng. Symp. Ser.*, vol. 86, no. 2, pp. 785-793, 1984. DOI: 10.1016/B978-0-85295-175-0.50013-8.
57. S. Grauso, R. Mastrullo, A. W. Mauro, and G. P. Vanoli, "Flow boiling of R410A and CO₂ from low to medium reduced pressures in macro channels: Experiments and assessment of prediction methods," *Int. J. Heat Mass Transfer*, vol. 56, no. 1 – 2. pp. 107-118, 2013. DOI: 10.1016/j.ijheatmasstransfer.2012.09.015.
58. R. Mastrullo, A. W. Mauro, A. Rosato, and G. P. Vanoli, "Carbon dioxide local heat transfer coefficients during flow boiling in a horizontal circular smooth tube," *Int. J. Heat Mass Transfer*, vol. 52, no. 19 – 20. pp. 4189-4194, 2009. DOI: 10.1016/j.ijheatmasstransfer.2009.04.004.
59. R. Mastrullo, A. W. Mauro, A. Rosato, and G. P. Vanoli, "Carbon dioxide heat transfer coefficients and pressure drops during flow boiling: Assessment of predictive methods," *Int. J. Refrig.*, vol. 33, no. 6, pp. 1068-1085, 2010. DOI: 10.1016/j.ijrefrig.2010.04.005.

60. J. Wu et al. , “Investigation of heat transfer and pressure drop of CO₂ two-phase flow in a horizontal minichannel,” *Int. J. Heat Mass Transfer*, vol. 54, no. 9 – 10, pp. 2154-2162, 2011. DOI: 10.1016/j.ijheatmasstransfer.2010.12.009.
61. L. Cheng, “Microscale and nanoscale thermal and fluid transport phenomena: Rapidly developing research fields,” *Int. J. Microscale Nanoscale Therm. Fluid Transp. Phenom.*, vol. 1, no. 1, pp. 3-6, 2010.
62. L. Cheng, and A. Ghajar, “Frontiers and progress in multiphase flow and heat transfer,” *Heat Transfer Eng.*, vol. 40, no. 16, pp. 1229-1300, 2019. DOI: 10.1080/01457632.2018.1470283.
63. G. Xia, B. Cai, L. Cheng, Zh. Wang, “Experimental study and modeling of average void fraction of gas-liquid two-phase flow in a horizontal helically coiled rectangular channel,” *Exp. Therm. Fluid Sci.*, vol. 94, pp. 9-22, Jun., 2018. DOI: 10.1016/j.expthermflusci.2018.01.027.
64. W. Qu, and I. Mudawar, “Measurement and correlation of critical heat flux in two-phase micro-channel heat sinks,” *Int. J. Heat Mass Transfer*, vol. 47, no. 10 – 11, pp. 2045 -2059, 2004. DOI: 10.1016/j.ijheatmasstransfer.2003.12.006
65. G. Wang, P. Cheng, and A.E. Bergles, “Effects of inlet/outlet configurations on flow boiling instability in parallel microchannels,” *Int. J. Heat and Transfer*, vol. 51, no. 9 – 11, pp. 2267–228, 2008. DOI: 10.1016/j.ijheatmasstransfer.2007.08.027.
66. G. Wang, P. Cheng, and H. Wu, “Unstable and stable flow boiling in parallel microchannel and in a single microchannel,” *Int. J. Heat Mass Transfer*, vol. 50, no. 21 – 22, (2007) 4297-4310. DOI: 10.1016/j.ijheatmasstransfer.2007.01.033.
67. G. Hetsroni, A. Mosyak, Z. Segal, and G. Ziskind, “A uniform temperature heat sink for cooling of electric devices,” *Int. J. Heat Mass Transfer*, vol. 45, no. 16, pp. 3275-3286, 2002. DOI: 10.1016/S0017-9310(02)00048-0.

68. H. Huang, N. Borhani, and J.R. Thome, “Thermal response of multi-microchannel evaporators during flow boiling of refrigerants under transient heat loads with flow visualization,” *J. Electron. Packag.*, vol. 128, no. 3, 031004, 13 pages, 2016. DOI: doi.org/10.1115/1.4033487.
69. G. Xia, M. Du, L. Cheng, and W. Wang, “Experimental study on the nucleate boiling heat transfer characteristics of a multi-wall carbon nanotubes water based nanofluid in a confined space,” *Int. J. Heat Mass Transfer*, vol. 113, pp. 59-16, Oct., 2017. DOI: 10.1016/j.ijheatmasstransfer.2017.05.021.
70. Y. Lv, G. Xia, L. Cheng, and D. Ma, “Experimental study on the pressure drop oscillation characteristics of the flow boiling instability with FC-72 in parallel rectangle microchannels,” *Int. Comm. Heat Mass Transfer*, vol. 108, 104289, 13 pages, Nov., 2019. DOI: 10.1016/j.icheatmasstransfer.2019.104289.
71. G. Xia, Y. Lv, L. Cheng, D. Ma, and Y. Jia, “Experimental study and dynamic simulation of the continuous two phase instable boiling in multiple parallel microchannels,” *Int. J. Heat Mass Transfer*, vol. 138, pp. 961-984, Aug., 2019. DOI: 10.1016/j.ijheatmasstransfer.2019.04.124.
72. L. Cheng, G. Xia, Q. Li, and J. R. Thome, “Fundamental issues, technology development and challenges of boiling heat transfer, critical heat flux and two-phase flow phenomena with nanofluids,” *Heat Transfer Eng.*, vol. 40, no. 16, pp. 1301-1336, 2019. DOI: 10.1080/01457632.2018.1470285.
73. G. Xia, Y. Cheng, L. Cheng, and Y. Li, “Heat transfer characteristics and flow visualization during flow boiling of acetone in semi-open multi-microchannels,” *Heat Transfer Eng.*, vol. 40, no. 16, pp. 1349-1362, 2019. DOI: 10.1080/01457632.2018.1470296.
74. J. Patiño et al. “A comparative analysis of a CO₂ evaporator model using experimental heat transfer correlations and a flow pattern map,” *Int. J. Heat Mass Transfer*, vol. 71, 361-375, Apr., 2014. DOI: 10.1016/j.ijheatmasstransfer.2013.12.027.

75. J. M. Marcinichen, J. R. Thome, and R. H. Pereira, "Working fluid charge reduction, part 1: CO₂ fin tube evaporator designed for light commercial appliances utilizing flow pattern based phenomenological prediction models," *Int. J. Refrig.*, vol. 65, pp. 258–272, May, 2016. DOI: 10.1016/j.ijrefrig.2015.12.017.
76. S. Yamaguchi, D. Kato, K. Saito, and S. Kawai, "Development and validation of static simulation model for CO₂ heat pump," *Int. J. Heat Mass Transfer*, vol. 54, no. 9 – 10, pp. 1896-1906, 2011. DOI: 10.1016/j.ijheatmasstransfer.2011.01.013.
77. S. Wang, H. Tuo, F. Cao, and Z. Xing, Z., "Experimental investigation on air-source transcritical CO₂ heat pump water heater system at a fixed water inlet temperature," *Int. J. Refrig.*, vol. 36, no. 3, pp. 701-716, 2013. DOI: 10.1016/j.ijrefrig.2012.10.011.
78. R. N. Faria, R. O. Nunes, R. N. N. Koury, and L. Machado, "Dynamic modeling study for a solar evaporator with expansion valve assembly of a transcritical CO₂ heat pump," *Int. J. Refrig.*, vol. 64, 203–213, Apr. 2016. DOI: 10.1016/j.ijrefrig.2016.01.004.
79. D. Yang, Y. Song, F. Cao, L. Jin, and X. Wang, "Theoretical and experimental investigation of a combined R134a and transcritical CO₂ heat pump for space heating," *Int. J. Refrig.*, vol. 72, pp. 156-170, Dec., 2016. DOI: 10.1016/j.ijrefrig.2016.07.016.
80. Z. Tong, X. H. Liu, Z. Li, and Y. Jiang, "Experimental study on the effect of fill ratio on an R744 two-phase thermosyphon loop," *Appl. Therm. Eng.*, vol. 99, pp. 302–312, Apr., 2016. DOI: 10.1016/j.applthermaleng.2016.01.065.
81. G. Xia, W. Wang, L. Cheng, and D. Ma, "Visualization study on the instabilities of phase-change heat transfer in a flat two-phase closed thermosyphon," *Appl. Therm. Eng.*, vol. 116, pp. 392-405, Apr., 2017. DOI: 10.1016/j.applthermaleng.2017.01.096.

82. S. Yoshioka, H. Y. Kim, and K. Kasai, "Heat transfer performance and oil behaviour for R744 with PAG oil in air-cooled heat exchanger," in: *Proc. 8th IIR Gustav Lorentzen Conf. Natural Working Fluids*, Copenhagen, September 7 - 10, 2008, pp. 389–396.
83. E. P Bandarra Filho, L. Cheng, and J. R Thome, "Flow boiling characteristics and flow pattern visualization of refrigerant/lubricant oil mixtures," *Int. J. Refrig.*, vol. 32, no. 2, pp. 185-202, 2009. <https://doi.org/10.1016/j.ijrefrig.2008.06.013>.

List of Figure Captions

Figure 1. Schematic of ammonia-CO₂ in secondary loop of an indirect refrigeration system.

Figure. 2. Schematic of CO₂ automobile air-conditioning system.

Figure 3. Pressure-enthalpy diagrams of CO₂ and R134a in automobile air-conditioning systems.

Figure 4. Comparison of the definitions of macro- and micro-scale channels for CO₂ according to Kandlikar [10] and the Confinement number Co [11].

Figure 5. The experimental heat transfer coefficients in two different studies showing two opposite trends with the increase of saturation temperature. Arrow 1 showing the trend of the experimental flow boiling heat transfer coefficients (solid symbols) of Pettersen [21]: $D_h = 0.8$ mm, $G = 280$ kg/m²s and $q = 10$ W/m² at 0, 20 and 25 °C. Arrow 2 showing the trend of the experimental flow boiling heat transfer coefficients (open symbols) of Yoon et al. [25]: $D_h = 7.53$ mm, $G = 318$ kg/m²s and $q = 16.4$ W/m² at 5, 15 and 20 °C.

Figure 6. The experimental flow boiling heat transfer coefficients in the same study showing different results with a very little change of hydraulic diameters from 1.53 mm to 1.54 mm. Solid symbols showing the experimental flow boiling heat transfer coefficients of Yun et al. [22]: $D_h = 1.53$ mm, $G = 300$ kg/m²s, $T_{sat} = 5$ °C and $q = 20$ W/m². Open symbols showing the experimental flow boiling

heat transfer coefficients of Yun et al. al. [22]: $D_h = 1.54$ mm, $G = 300$ kg/m²s, $T_{sat} = 5$ °C and $q = 20$ W/m².

Figure 7. Schematic diagram of film thickness.

Figure 8. (a) Comparison of the predicted flow boiling heat transfer coefficients (solid line showing the predicted heat transfer coefficients) to the experimental data (* symbols showing the measured data points) of Yun et al. [26]; (b) the corresponding flow pattern map (* symbols showing the measured data points) at the test conditions: $D_{eq} = 2$ mm, $q = 30$ kW/m², $T_{sat} = 5$ °C and $G = 1500$ kg/m²s.

Figure 9. Simulation of flow boiling model and flow pattern map.

(a) For 1.15 mm channel at the conditions: $q = 11$ kW/m², $T_{sat} = 10$ °C and $G = 300$ kg/m²s with indicated value at $x = 0.30$; (b) For 3 mm channel at the conditions: $q = 20$ kW/m², $T_{sat} = 10$ °C and $G = 390$ kg/m²s with indicated value at $x = 0.70$.

Figure 10. The effects of stable and instable boiling on the fluid and wall temperature [71].

(a) The variation of the fluid temperature with time for both stable and unstable flow boiling at the working conditions of $G_{in} = 868.3$ kg/m²s, $q_{eff} = 57.5$ W/cm² and $T_{in} = 28$ °C; (b) The wall temperature difference between the subcooled region and saturated region at stable states, and the mass fluxes are 437.2 kg/m²s, 607.6 kg/m²s and 868.1 kg/m²s respectively.

Figure 11. System flow diagram of CO₂ heat pump and measuring points in the study of Yamaguchi et al. [76].

Figure 12. Schematic diagram of the CO₂ Evaporator the study of Yamaguchi et al. [76].

Figure 13. The effect of the water inlet temperature the COP and heat flow rate [76].

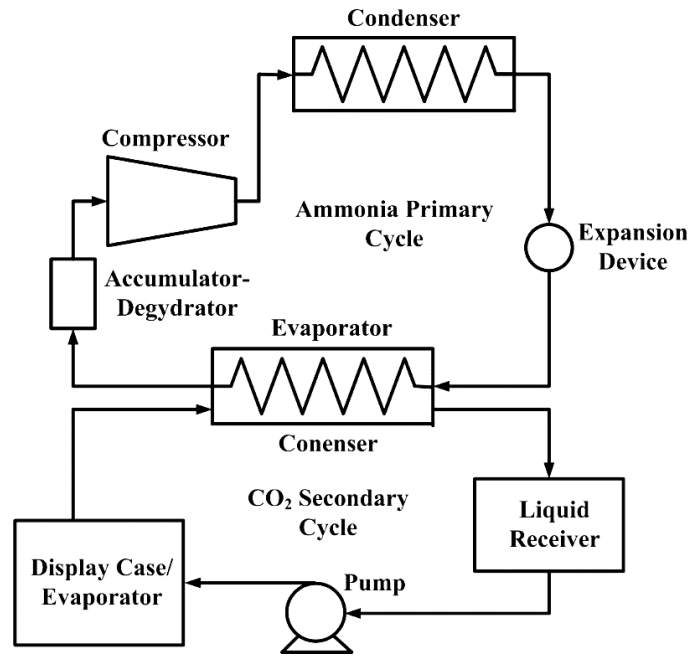


Figure 1. Schematic of ammonia-CO₂ in secondary loop of an indirect refrigeration system.

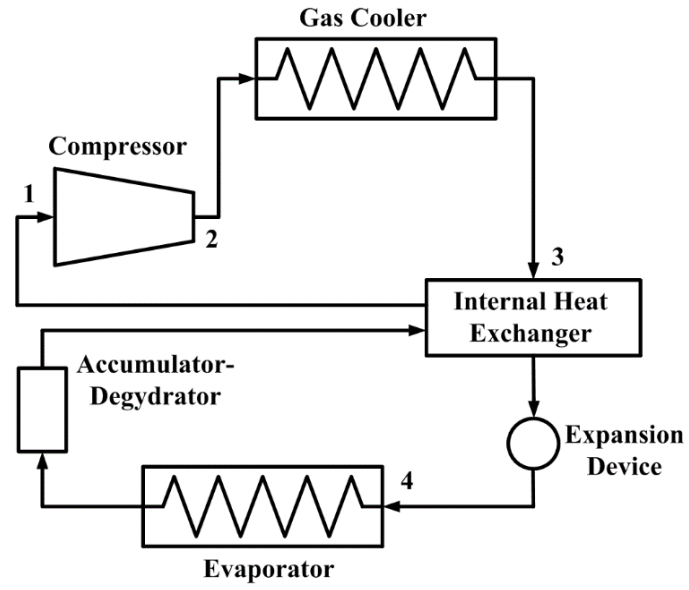


Figure. 2. Schematic of CO₂ automobile air-conditioning system.

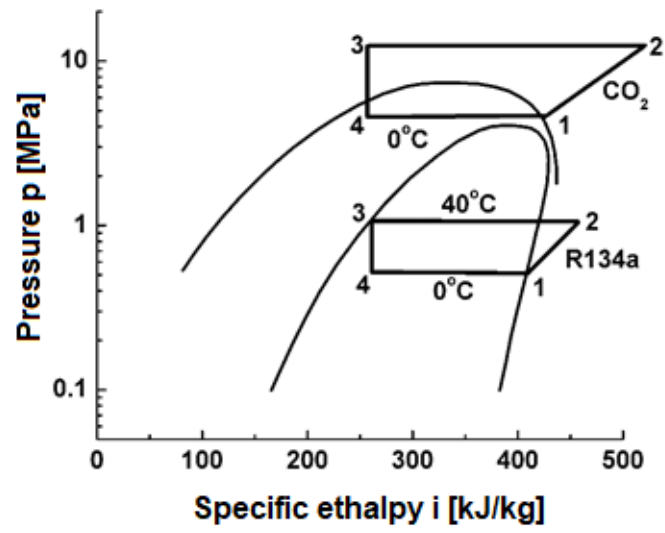


Figure 3. Pressure-enthalpy diagrams of CO_2 and R134a in automobile air-conditioning systems.

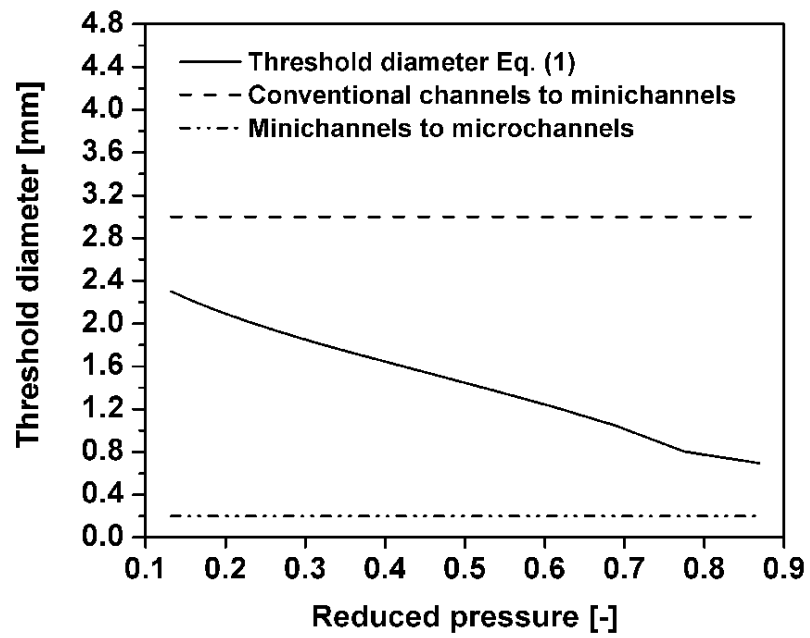


Figure 4. Comparison of the definitions of macro- and micro-scale channels for CO₂ according to Kandlikar [10] and the Confinement number Co [11].

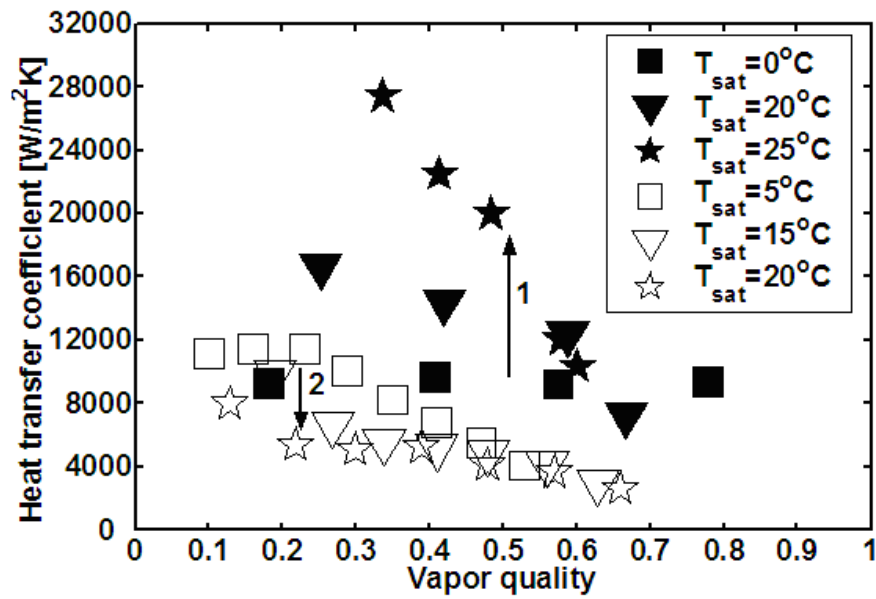


Figure 5. The experimental heat transfer coefficients in two different studies showing two opposite trends with the increase of saturation temperature. Arrow 1 showing the trend of the experimental flow boiling heat transfer coefficients (solid symbols) of Pettersen [21]: $D_h = 0.8$ mm, $G = 280$ kg/m²s and $q = 10$ W/m² at 0, 20 and 25 °C. Arrow 2 showing the trend of the experimental flow boiling heat transfer coefficients (open symbols) of Yoon et al. [25]: $D_h = 7.53$ mm, $G = 318$ kg/m²s and $q = 16.4$ W/m² at 5, 15 and 20 °C.

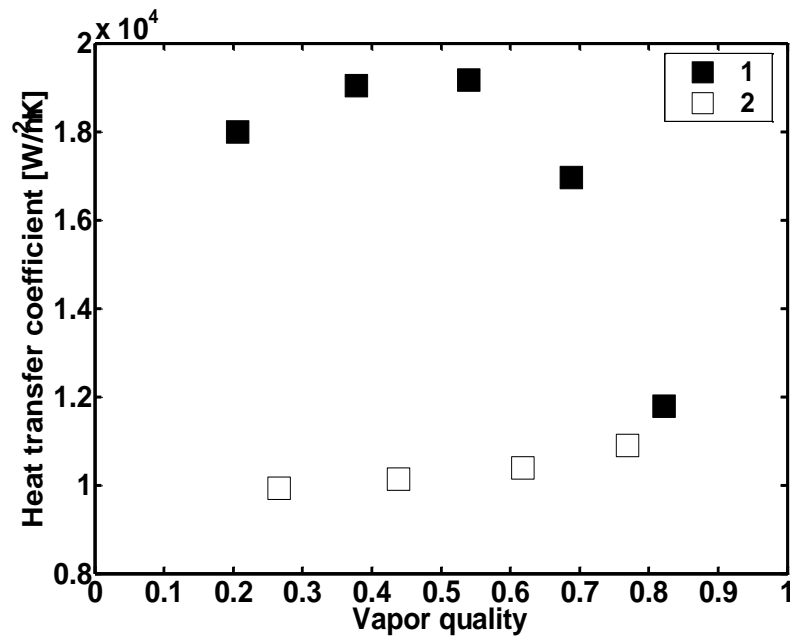


Figure 6. The experimental flow boiling heat transfer coefficients in the same study showing different results with a very little change of hydraulic diameters from 1.53 mm to 1.54 mm. Solid symbols showing the experimental flow boiling heat transfer coefficients of Yun et al. [22]: $D_h = 1.53$ mm, $G = 300$ kg/m²s, $T_{sat} = 5$ °C and $q = 20$ W/m². Open symbols showing the experimental flow boiling heat transfer coefficients of Yun et al. al. [22]: $D_h = 1.54$ mm, $G = 300$ kg/m²s, $T_{sat} = 5$ °C and $q = 20$ W/m².

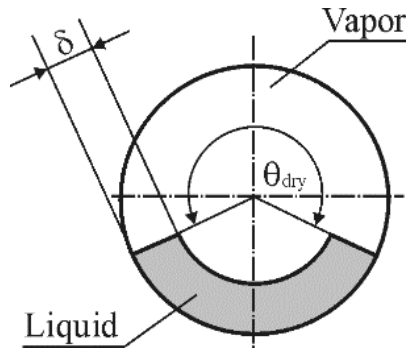
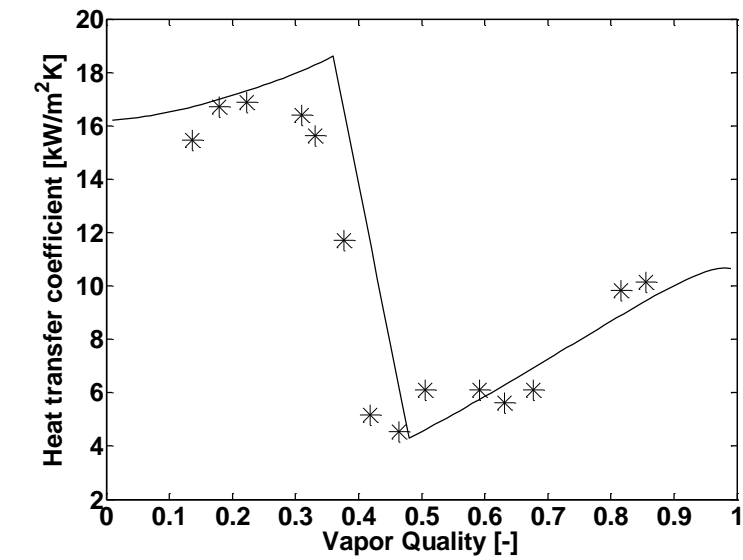
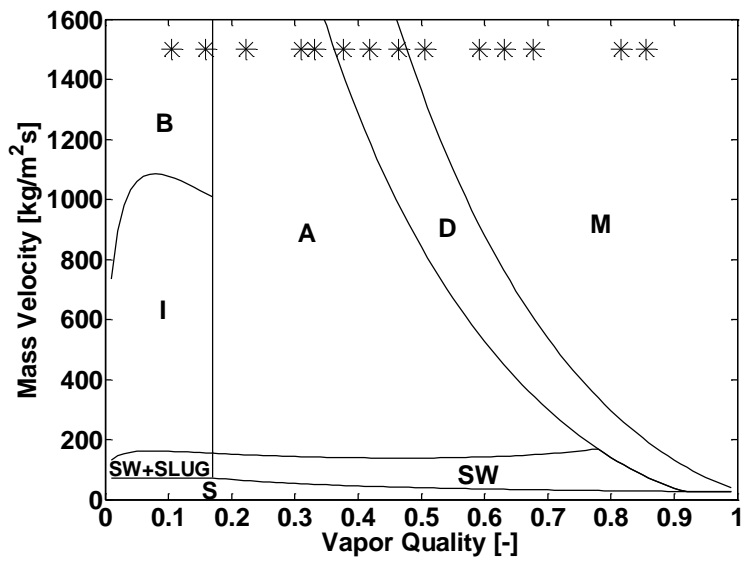


Figure 7. Schematic diagram of film thickness.

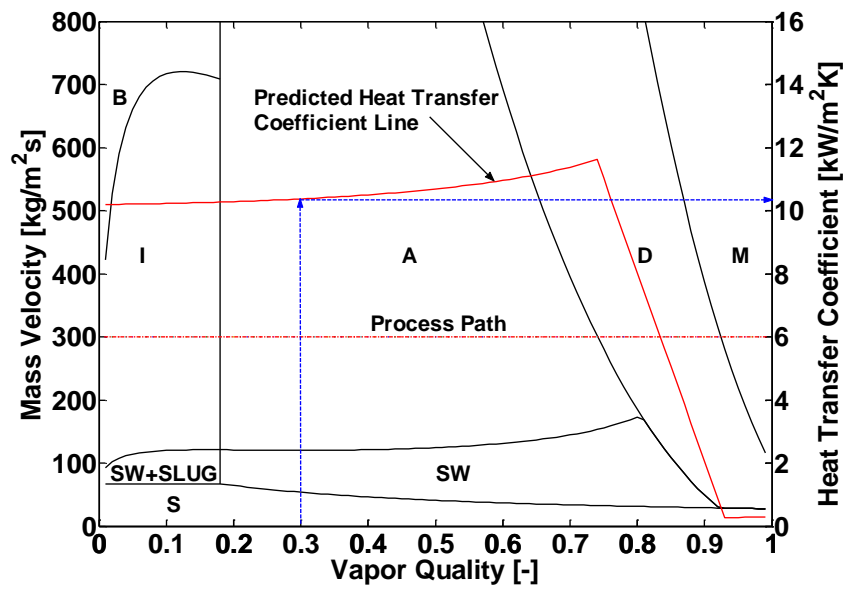


(a)

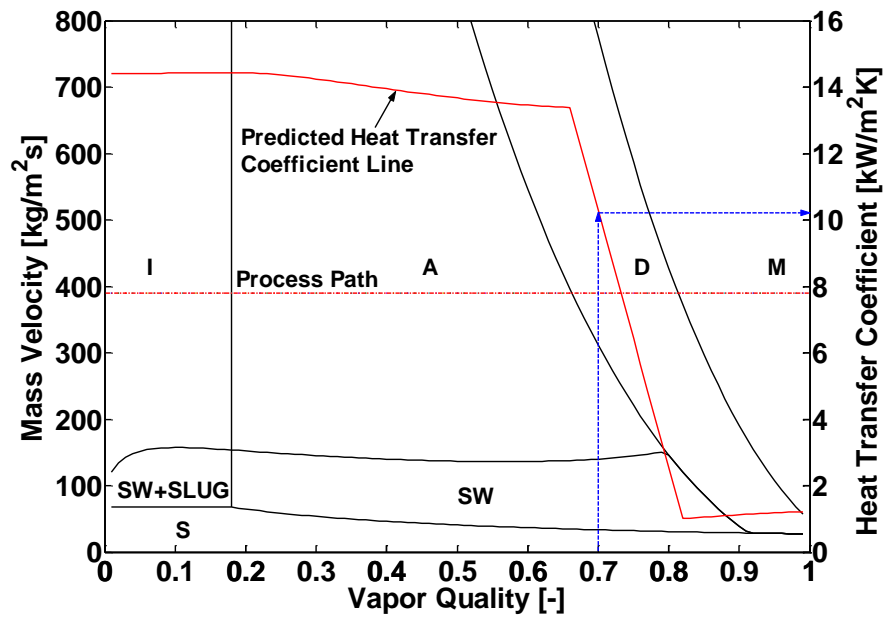


(b)

Figure 8. (a) Comparison of the predicted flow boiling heat transfer coefficients (solid line showing the predicted heat transfer coefficients) to the experimental data (* symbols showing the measured data points) of Yun et al. [26]; (b) the corresponding flow pattern map (* symbols showing the measured data points) at the test conditions: $D_{eq} = 2 \text{ mm}$, $q = 30 \text{ kW/m}^2$, $T_{sat} = 5^\circ\text{C}$ and $G = 1500 \text{ kg/m}^2\text{s}$.



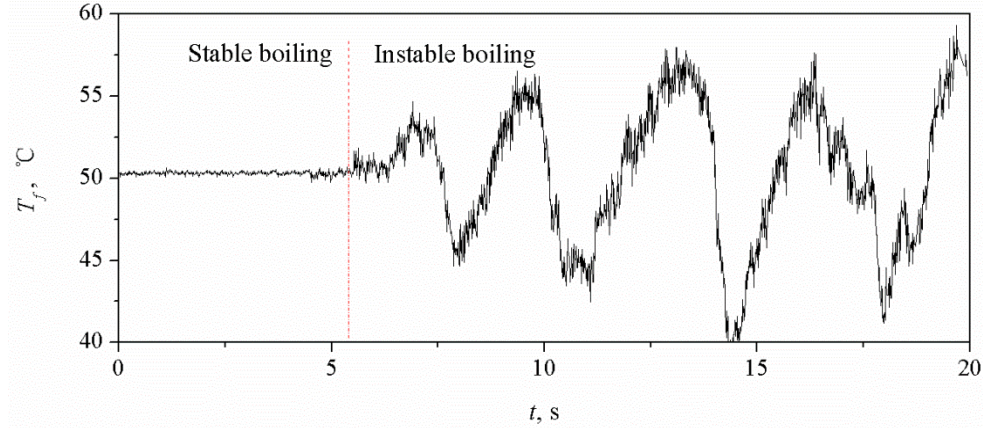
(a)



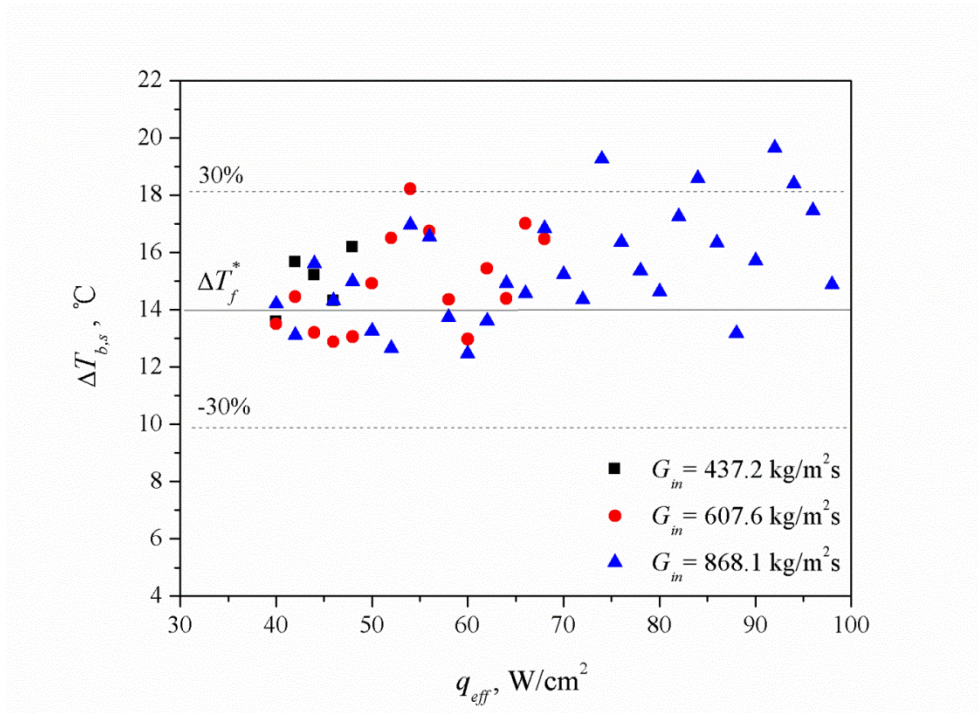
(b)

Figure 9. Simulation of flow boiling model and flow pattern map.

(a) For 1.15 mm channel at the conditions: $q = 11 \text{ kW/m}^2$, $T_{sat} = 10^\circ\text{C}$ and $G = 300 \text{ kg/m}^2\text{s}$ with indicated value at $x = 0.30$; (b) For 3 mm channel at the conditions: $q = 20 \text{ kW/m}^2$, $T_{sat} = 10^\circ\text{C}$ and $G = 390 \text{ kg/m}^2\text{s}$ with indicated value at $x = 0.70$.



(a)



(b)

Figure 10. The effects of stable and unstable boiling on the fluid and wall temperature [71].

(a) The variation of the fluid temperature with time for both stable and unstable flow boiling at the working conditions of $G_{in} = 868.3 \text{ kg/m}^2\text{s}$, $q_{eff} = 57.5 \text{ W/cm}^2$ and $T_{in} = 28^\circ\text{C}$; (b) The wall temperature difference between the subcooled region and saturated region at stable states, and the mass fluxes are $437.2 \text{ kg/m}^2\text{s}$, $607.6 \text{ kg/m}^2\text{s}$ and $868.1 \text{ kg/m}^2\text{s}$ respectively.

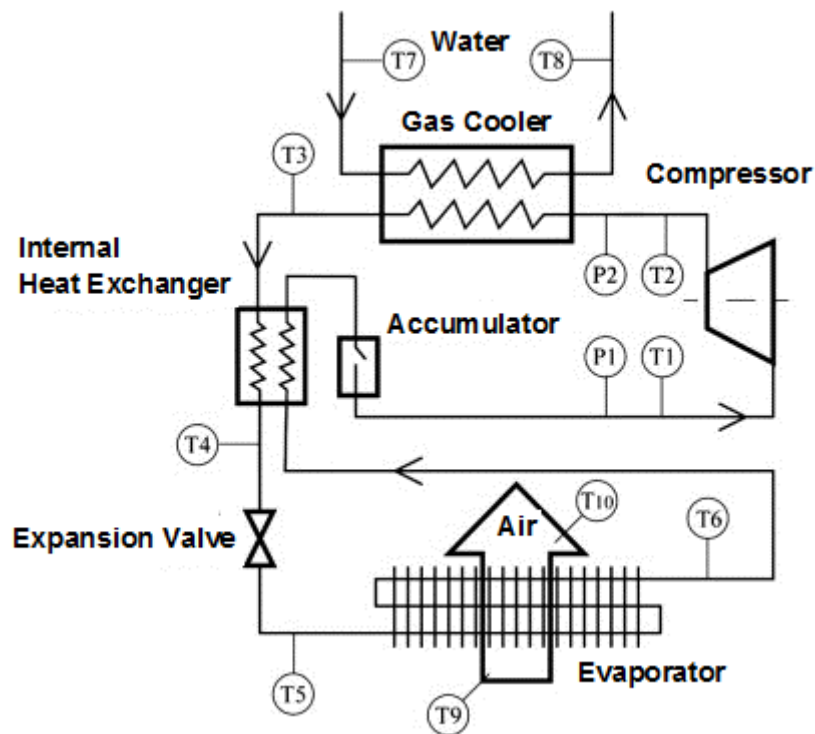


Figure 11. System flow diagram of CO₂ heat pump and measuring points in the study of Yamaguchi et al. [76].

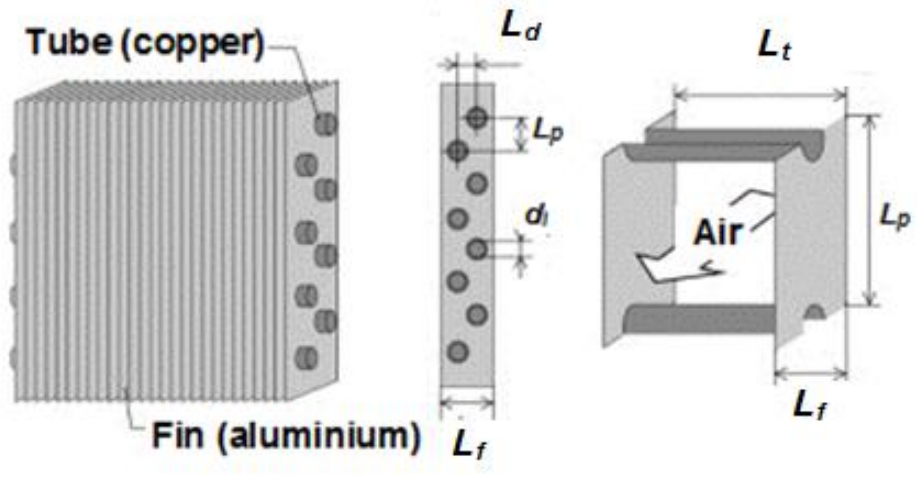


Figure 12. Schematic diagram of the CO₂ Evaporator the study of Yamaguchi et al. [76].

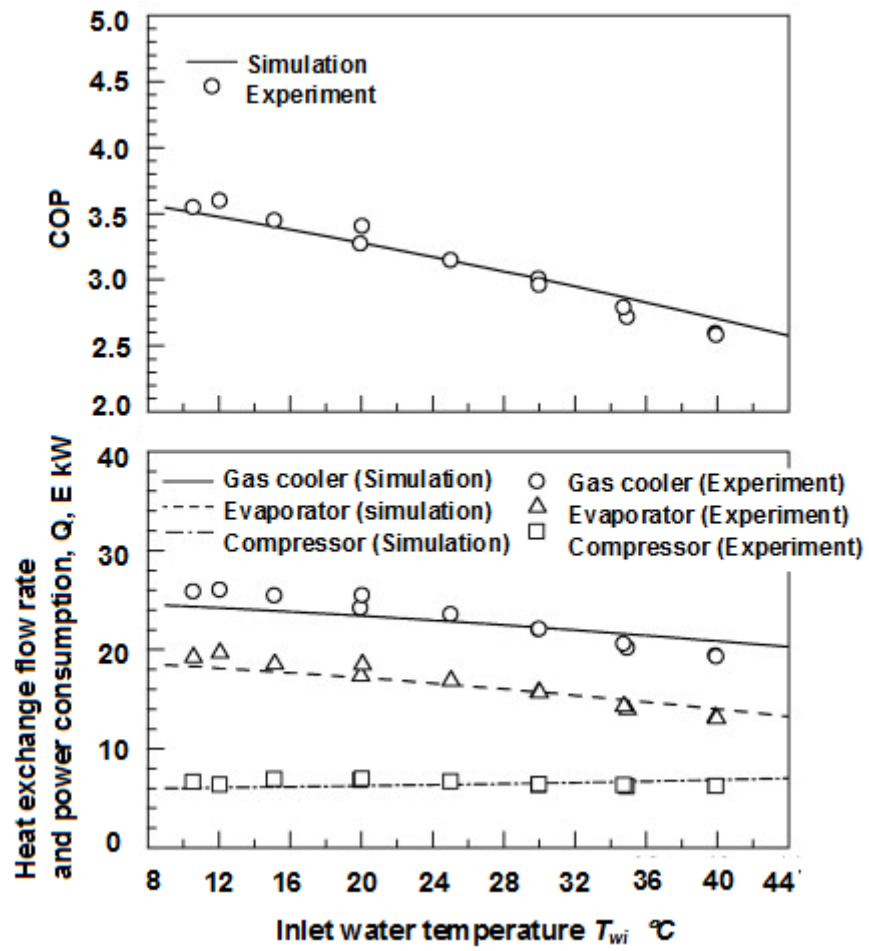


Figure 13. The effect of the water inlet temperature on the COP and heat flow rate [76].

Notes on contributors



Lixin Cheng has worked at Sheffield Hallam University since 2016. He obtained his Ph.D. in Thermal Energy Engineering at the State Key Laboratory of Multiphase Flow at Xi'an Jiaotong University, China in 1998. He has received several prestigious awards such as Alexander von Humboldt Fellowship in Germany in 2006, an ERCOFTAC Visitor Grant in Switzerland in 2010 and a Distinguished Visiting Professorship of the City of Beijing, China in 2015. His research interests are multiphase flow and heat transfer and thermal energy engineering. He has published more than 100 papers in journals and conferences, 9 book chapters and edited 10 books. He has delivered more than 60 keynote and invited lectures worldwide. He has been the chair of the *World Congress on Momentum, Heat and Mass Transfer (MHMT)* since 2017. He is one of the founders and co-chair of the *International Symposium of Thermal-Fluid Dynamics (ISTFD)* series since 2019. He is associate editor of *Heat Transfer Engineering* and *Journal of Fluid Flow, Heat and Mass Transfer*, and international advisor of *Thermal Power Generation* (a Chinese journal).



Guodong Xia is a leading professor in Thermal Energy Engineering at Beijing University of Technology, China. He received his Ph.D. in Thermal Energy Engineering at the State Key Laboratory of Multiphase Flow of Xi'an Jiaotong University, China in 1996. He was a visiting professor in the Institute of Process Engineering at the University of Hanover, Germany in 2000 -2001. His research interests include fundamentals and applications of microscale heat transfer, multiphase flow and heat transfer, waste energy recovery, thermal energy system, heat exchanger design and enhanced heat transfer. He is a member of the multiphase flow committee of the Chinese

Society of Engineering Thermophysics and a member of the multiphase flow committee of the Chinese Society of Theoretical and Applied Mechanics. He has published more than 150 papers in journals and conferences.



Qinling Li is a senior lecturer in the Department of Engineering and Mathematics, Sheffield Hallam University, UK. After received her PhD in the School of Engineering & Science, University of Southampton, she worked as research associate on two EPSRC projects, one in Aeronautical and Automatics Engineering Department, Loughborough University (2003 - 2006), another one in the Department of Applied Mathematics and Theoretical Physics, University of Cambridge (2006 - 2009). Her main research fields are fundamentals of compressible turbulence, shock-waves boundary layer interaction, jet-in-cross flow & mixing enhancement, turbine/combustion chamber cooling effectiveness, fan broadband noise prediction, short take-off and vertical landing aircraft (STOVL) in the descending phase, high-order numerical methods used in DNS/LES, fluid-structure interaction, nanofluids and microscale fluid/heat transfer. She has published over 20 peer-reviewed publications (book/book chapters, journals and conferences).